Microscopic study of electromagnetic properties and band spectra of neutron deficient ^{133,135,137}Sm

Rakesh K. Pandit[1] R.K. Bhat[1] Rani Devi[2;1)] S.K. Khosa[3] G.H. Bhat[4] J.A. Sheikh[5]

[1]Department of Higher Education, Government of J&K, Jammu and Kashmir, India
[2]Department of Physics, University of Jammu, Jammu- 180006, India
[3]Department of Physics and Astronomical Sciences, Central University of Jammu, Jammu- 181143, India
[4]Department of Physics, SP College, Cluster University Srinagar- 190001, India
[5]Cluster University Srinagar - Jammu and Kashmir 190001, India

Abstract: A microscopic high spin study of neutron deficient and normally deformed ^{133,135,137}Sm has been carried out in projected shell model framework. The theoretical results have been obtained for the spins, parities and energy values of yrast and excited bands. Besides this, the band spectra, band head energies, moment of inertia and electromagnetic transition strengths are also predicted in these isotopes. The calculations successfully give a deeper understanding of the mechanism of the formation of yrast and excited bands from the single and multi-quasi particle configurations. The results on moment of inertia predict an alignment of a pair of protons in the proton $(1h_{11/2})^2$ orbitals in the yrast ground state bands of $^{133\text{-}137}$Sm due to the crossing of one quasiparticle bands by multi-quasiparticle bands at higher spins. The discussion in the present work is based on the deformed single particle scheme. Any future experimental confirmation or refutation of our predictions will be a valuable information which can help to understand the deformed single particle structure in these odd mass neutron deficient $^{133\text{-}137}$Sm.

Keywords: projected shell model, Sm isotopes, band spectra

PACS: 21.60.-n, 21.10.-ky, 27.60.+j **DOI:** 10.1088/1674-1137/43/12/124108

1 Introduction

The study of neutron deficient nuclei in the mass region A~130 has been an interesting subject in the nuclear structure physics [1], as this region provides an opportunity to test nuclear models. For the neutron deficient nuclei in this mass region, it is known that the proton Fermi surface lies in lower part of the $h_{11/2}$ sub-shell which suggests a T=0 driving force for the onset of collective prolate shape. Wadsworth et al. [2] have presented the first evidence for the occurrence of $vi_{13/2}[660]1/2^+$ neutron band in ^{133}Sm isotope. This was in fact the first observation of the occupation of this orbital in a nucleus with N<73. Later Regan et al. [3] have investigated the low lying rotational band structures of ^{133}Sm using the ^{40}Ca+ ^{96}Ru reaction at a beam energy of approximately 180 MeV and observed five new bands in ^{133}Sm, out of which two are strongly coupled bands predicted to be built upon Nilsson configurations $vh_{11/2}[523]7/2^-$ and $vd_{5/2}[402]5/2^+$. They also have found evidence for a second decoupled band built upon a single $h_{9/2}[541]1/2^-$ orbital, in addition to the previously reported $vi_{13/2}$ intruder band [2]. Parry et al. [4] have studied high spin states of ^{133}Sm via the ^{96}Ru (^{40}Ca, 2pn) reaction and studied rotational structures and their characteristics. They discovered new coupled band in ^{133}Sm that leads to the reassignment of the configuration of one of the previously [2,3] identified bands. The calculations of Parry et al. [4] predict strong polarization effects for different configurations which result in quadrupole deformations that vary from $\beta_2 \sim 0.28$ to $\geqslant 0.38$. In addition, Parry et al. [4] have identified a new band which appears to be the signature partner to previously [3] assigned decoupled band based on configuration $vi_{13/2}[600]1/2^+$.

Mullins et al. [5] was the first to propose the low level scheme of ^{135}Sm. They have identified the yrast band composed of α=−1/2 and α=+1/2 signatures of the $1vg_{7/2}$ band. They have also proposed the possibility for the band head spin of this yrast band at $I^\pi = 7/2^+$. Furthermore, they proposed the negative parity band to be based on a neutron in the $h_{11/2}$ orbital. The α=−1/2 component of this

Received 18 March 2019, Revised 24 September 2019, Published online 13 November 2019

1) E-mail: rani_rakwal@yahoo.co.in, corresponding author

negative parity band comes lower in energy. The α=+1/2 signature component of this band has been identified as much weaker signature. The authors of Ref. [5] have proposed the band head spin of this negative parity band at $I^{\pi}=9/2^{-}$.

In case of ^{137}Sm, the yrast band is based on a coupled neutron orbital from the upper $h_{11/2}$ mid-shell [6], and built on the [514]9/2^{-} Nilsson orbital. Both signature components of this orbital were observed in this nucleus. Paul et al. [7] have predicted deformation for this single $h_{11/2}$ quasi-neutron state as ε_2~0.20 and ε_4~0.026. Later on Alvarez et al. [8] have identified a positive parity band based on Nilsson configuration [400]1/2^{+} in ^{137}Sm.

After analyzing the literature, it is found that no single theoretical framework has been used in the past to study the band spectra in all the odd mass ^{133,135,137}Sm. Moreover, it is desired that odd mass Sm nuclei can be consistently described alongside even even Sm isotopes [9,10], which is a strict test for microscopic models. In the present work, an attempt has been made to study spectroscopic properties of $^{133\text{-}137}$Sm isotopes by using projected shell model and to reproduce the ground state band, excited bands, their relative band head energies, transition energies between two angular momentum states and electromagnetic transition strengths. Further, it is of interest to determine the extent to which the present calculation can account for the ground state and excited state deformations of $^{133\text{-}137}$Sm isotopes by using projected shell model. In this model, both pairing and deformation are treated self consistently. The pairing interaction is extended to incorporate both monopole and quadrupole terms. Therefore, it is necessary to test this model in a wider context within this mass region A~130-140 and also to investigate the role of proton configurations at higher spins.

The structure of the paper is as follows. In Section 2, a brief outline of the projected shell model is given. Results for calculated energy level schemes, transition energies between two angular momentum states, kinetic moment of inertia and discussion on band diagrams are presented in Section 3. Section 4 deals with the electromagnetic transition strength ratios for the yrast bands of $^{133\text{-}137}$Sm isotopes. In Section 5, the work is summarized and the conclusions are presented.

2 Calculational framework

Projected Shell Model [11] is basically a shell model developed for medium and heavy nuclear systems. It was designed to overcome the difficulties of the spherical shell model. In medium and heavy deformed nuclei, applying spherical shell model becomes unfeasible because of large dimensionality and its related problems. For such systems Hara and Sun [11] used deformed basis and the projected technique. A Fortran Code of projected shell model [12] was also developed later for carrying out calculations even on any modern PC, without any difficulties. In recent past, Sun [13] in his review article of PSM demonstrated how heavy deformed nuclei can be effectively explained with different truncation schemes.

2.1 Brief outline of the calculational framework

In this section, a brief introduction of the theory is presented. The complete description of the theory is given in the Refs. [11-18]. The projected shell model builds its model basis by using deformed quasiparticle-basis (qp), but selection of deformed basis involves violation of rotational symmetry of wave functions. The broken rotational symmetry in the wavefunction is restored by angular momentum projection technique [19]. The PSM, wavefunction can be written as

$$|\sigma, IM\rangle = \sum_{K\kappa} f^{\sigma}_{IK\kappa} \hat{P}^{I}_{MK} |\varphi_{\kappa}\rangle, \tag{1}$$

where $|\varphi_{\kappa}\rangle$ denotes the qp-basis, the index σ labels the states with the same angular momentum and κ labels the basis states. For the present calculations, the qp configurations for odd neutron nuclei are taken to be

$$|\varphi_{\kappa}\rangle = a^{\dagger}_{\nu}|0\rangle, a^{\dagger}_{\nu}a^{\dagger}_{\pi 1}a^{\dagger}_{\pi 2}|0\rangle. \tag{2}$$

The chosen energy window around the Fermi surface gives rise to a basis space, $|\varphi_{\kappa}\rangle$ in Eq. (2) of the order of 37. In the Eq. (1), $\hat{P}^{I}_{MK}$ is the angular momentum projection operator [19], which projects out from the intrinsic configuration $|\varphi_{\kappa}\rangle$ states with good angular momentum and $f^{\sigma}_{IK\kappa}$ are the weights of the basis states. The weights $f^{\sigma}_{IK\kappa}$ are determined by the diagonalization of the Hamiltonian H^{I}, in the space spanned by the states of Eq. (1). This leads to the eigen value equation

$$\sum_{K'\kappa'} \left(H^{I}_{K\kappa,K'\kappa'} - E^{\sigma}_{I} N^{I}_{K\kappa,K'\kappa'} \right) f^{\sigma}_{IK'\kappa'} = 0 \tag{3}$$

with a normalization condition

$$\sum_{K\kappa K'\kappa'} f^{\sigma}_{IK\kappa} N^{I}_{K\kappa,K'\kappa'} f^{\sigma'}_{IK'\kappa'} = \delta_{\sigma\sigma'}, \tag{4}$$

where $H^{I}_{K\kappa,K'\kappa'}$ and $N^{I}_{K\kappa,K'\kappa'}$ are, respectively the matrix elements of the Hamiltonian and the norm. The projection of an intrinsic state $|\varphi_{\kappa}\rangle$ onto a good angular momentum generates a rotational energy given by

$$E_{\kappa}(I) = \frac{\langle \varphi_{\kappa} | \hat{H} \hat{P}^{I}_{KK} | \varphi_{\kappa} \rangle}{\langle \varphi_{\kappa} | \hat{P}^{I}_{KK} | \varphi_{\kappa} \rangle} = \frac{H^{I}_{K\kappa K'\kappa'}}{N^{I}_{K\kappa K'\kappa'}}. \tag{5}$$

The above equation represents expectation value of the

Hamiltonian with respect to a projected multi-qp state κ.

The total Hamiltonian in the present study is of the form

$$\hat{H} = \hat{H}_0 - \frac{1}{2}\chi \sum_{\mu} \hat{Q}^{\dagger}_{2\mu}\hat{Q}_{2\mu} - G_M\hat{P}^{\dagger}\hat{P} - G_Q \sum_{\mu} \hat{P}^{\dagger}_{2\mu}\hat{P}_{2\mu}. \quad (6)$$

In the above equation $\hat{H}_0$ is spherical single particle Hamiltonian. The strength χ of the quadrupole-quadrupole (QQ) interaction is related to the quadrupole deformation [11] and is adjusted such that the measured quadrupole deformation parameter (ε_2) is obtained [20] as a result of the HFB self-consistent method [11,21,22]. In the present case, the valence space of the PSM includes three major harmonic oscillator shells with N= 3,4,5 for protons and 4,5,6 for neutrons. The Nilsson parameters κ and μ for these major harmonic oscillator shells are taken from the Ref. [23] for ^{133,135,137}Sm isotopes. Table 1, represents the quadrupole (ε_2) and hexadecapole (ε_4) deformation parameters [24,25] used for both positive as well as negative parity bands of $^{133\text{-}137}$Sm.

The Nilsson diagram obtained for neutrons by taking Nilsson parameters of [23] for quadrupole deformations (ε_2) is displayed in Fig. 1. In this Fig., the positive parity and negative parity states are represented by solid and dotted lines, respectively. The states in the dotted rectangle represent the range of Nilsson states near the fermi surface and range of deformation ε_2=0.20−0.33 within which the $^{133\text{-}137}$Sm isotopes lie. It can be seen from Fig.1,

Table 1. Deformation parameters used for both positive and negative parity bands of $^{133-137}$Sm.

Nuclei	^{133}Sm	^{135}Sm	^{137}Sm
ε_2	0.330	0.275	0.20
ε_4	0.035	0.070	0.04

that the positive parity K=5/2 from $2d_{5/2}$; K=3/2,5/2,7/2 from $1g_{7/2}$; K=1/2,3/2 from $2d_{3/2}$; K=1/2 from $3s_{1/2}$, orbitals and negative parity, K=3/2,5/2,7/2/,9/2 from $1h_{11/2}$; K=1/2 from $2f_{7/2}$,$1h_{9/2}$ orbitals lie inside the rectangle in the deformation range 0.20−0.33 for normally deformed bands of $^{133-137}$Sm. However, beyond ε_2 =0.36, K=1/2 from $i_{13/2}$ orbital crosses the K=5/2,7/2 from the $1g_{7/2}$ orbital. In the present work, the normally deformed bands from the N=4 and 5 oscillator shells, that lie in the range ε_2=0.20-0.33 of deformation in $^{133-137}$Sm are discussed. The highly deformed (HD) and super deformed (SD) neutron [660]1/2^{+} ($vi_{13/2}$) bands [4,5,8,26,27] appear at enhanced quadrupole deformations and are not studied here due to the limitation of present calculations.

The monopole pairing interaction constant G_M is taken as

$$G_M = \left(G_1 \mp G_2\frac{N-Z}{A}\right)\frac{1}{A}\ \text{MeV}, \quad (7)$$

where minus (plus) sign is for neutrons (protons). The G_M is adjusted via G_1 and G_2 and their values are taken as

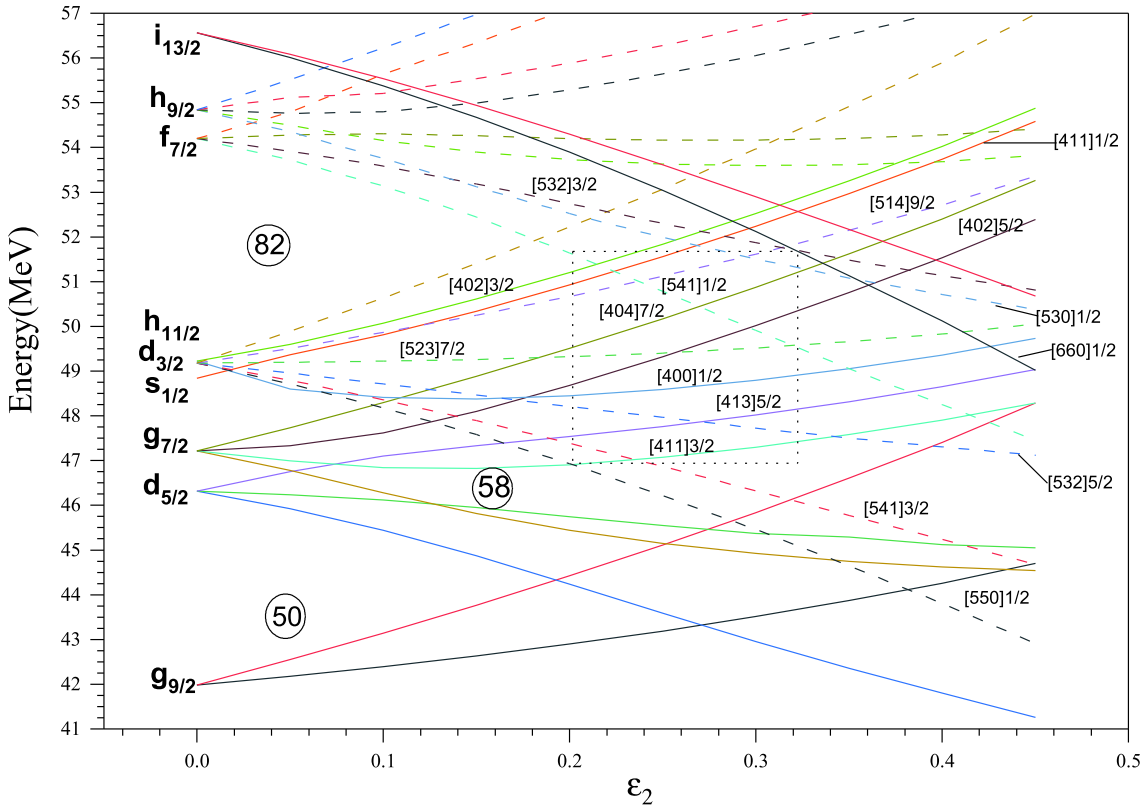

Fig. 1. (color online) The Nilsson diagram for neutrons, obtained by using Nilsson parameters of Ref. [23].

19.60 and 13.60, for the calculation of $^{133\text{-}137}$Sm isotopes. The quadrupole pairing strength G_Q is proportional to G_M with a proportionality constant (γ) taken as 0.16 (positive parity) and 0.28 (negative parity) for ^{133}Sm, 0.28 (positive parity) and 0.20 (negative parity) for ^{135}Sm, and 0.24 for ^{137}Sm. The odd mass nuclei are more sensitive to single particle states as compared to even-even nuclei due to the occupation of different single particle orbitals. For example, the ground state of ^{133}Sm arises from $5/2^+[413]$ neutron configuration but with the addition of four neutrons the ground state of ^{137}Sm arises from $9/2^-[514]$ neutron configuration. Therefore, γ parameter has been adjusted to reproduce the band head spin, energies and crossings of 1-qp band by 3-qp bands [22]. In case of ^{133}Sm, the positive parity band is the ground state band and the relative band head energy of negative parity yrast band is not known experimentally, therefore, to get the positive value of band head energy of negative parity bands, γ has been fixed as 0.28. For ^{135}Sm, the experimental band head energies of yrast positive and negative parity bands are not known. In this nucleus for delaying the crossing of 1-qp (quasiparticle) bands by 3-qp bands, the value of γ has been fixed as 0.28 for positive parity bands and 0.20 for negative parity bands.

3 Results and discussions

3.1 ^{133}Sm

Experimentally seven energy bands have been identified in this nucleus, out of which six are coupled bands designated as bands 1,2; 3,4; 5,6 and a decoupled band 7 [4]. Two bands are said to be coupled if they are linked with each other by dipole transitions $M1$. In case of ^{133}Sm, band 7 is isolated and is not connected with any other neighboring band and therefore is called a decoupled band. The two pairs of bands 1,2 and 5,6 are strongly coupled bands, as indicated by large experimental $B(M1)/B(E2)$ ratios [4] for the low spin transitions in the two pairs of bands. In the case of decoupled bands, $M1/E2$ transitions are either absent or weak, depending on the amount of decoupling. Two pairs of bands 1,2 and 3,4 are of positive parity and three bands 5,6 and 7 are of negative parity.

3.1.1 Strongly coupled bands 1 and 2

The band spectra for ^{133}Sm nucleus have been obtained with quadrupole and hexadecapole deformation parameters ε_2=0.330 and ε_4=0.035 for all the bands of ^{133}Sm. These values of deformation parameters are close to the values of 0.31 and 0.040, predicted for this nucleus by the authors of Ref. [24]. The calculations of Ref. [4] suggest a quadrupole deformation of 0.33 for the decoupled band 7 of ^{133}Sm. Therefore, to obtain all the bands 1-7 of ^{133}Sm, the value of ε_2 is chosen as 0.33. In a band diagram [11], rotational behavior of each configuration as well as its relative energy compared to other configurations is easily visualized. In these band diagrams, only low-lying projected bands are shown as the essence of physics of interest is satisfactorily reflected from these low-lying bands.

In Fig. 2, we plot the relevant low lying 1-qp and 3-qp positive parity bands in ^{133}Sm, along with their configurations. From the Fig. 2, it is seen that 1-qp neutron band built on K=5/2 and having configuration $1\nu 5/2^+[413]$ ($2d_{5/2}$), is lowest in energy up to the spin $(I) = 31/2^+$.

Experimentally, bands 1 and 2 shown in Fig. 3 are lowest positive parity energy bands available for comparison with theoretical results. We can, therefore, identify them with the bands obtained by us theoretically. The calculated results also support and are consistent with the band head spin and configuration assigned to the lowest positive parity band built on K=5/2 by the authors of Refs. [3,4]. Also, from the comparison of calculated and experimental energy spectra given in Fig. 3, it is clear that the agreement between calculated and experimental spectra [4,28] of band 1 and 2 (α=±1/2) is reasonably good. The difference between calculated and experimental values at the highest known spin $I=29/2^+$ (α=+1/2) of band 1 is 0.261 MeV and the difference at the highest known spin $I=27/2^+$ (α=−1/2) of band 2 is 0.293 MeV. At spin $33/2^+$, this ground state band is crossed by two 3-qp bands (as shown in the band diagram of Fig.2). This crossing by 3-qp bands causes a significant change in the yrast structure from $33/2^+$ onwards. The yrast states from $33/2^+$ onwards are predicted to arise from the superposition of two 3-qp bands having configurations $1\nu 5/2^+[413]+\{1\pi 3/2^-[541]+1\pi 5/2^-[532]\}$, K=7/2 and $1\nu 1/2^+[400]+\{1\pi 3/2^-[541]+1\pi 5/2^-[532]\}$, K=3/2.

3.1.1.1 Kinetic moment of inertia of bands 1 and 2

Rotational spectra in deformed nuclei can be better discussed in terms of moment of inertia. It is well known that the moment of inertia is sensitive to nuclear properties, like the pairing strength and the specific orbitals active at the Fermi surface. As moment of inertia depends upon the angular momentum, therefore its variation can impart some valuable information about the change in nuclear structure. Back-bending in moment of inertia can be calculated by using the formulae given in Ref. [29] and is a well-known phenomenon in understanding the nuclear structure at high-spins, which is expected to occur in rotating nuclei.

Calculated results on kinetic moment of inertia of bands 1-7 of ^{133}Sm are displayed in Fig. 4.

The calculated results on back-bending phenomenon in bands 1 and 2, based on the calculation of the kinematic moment of inertia $J^{(1)}$ and the rotational frequency (ω) are compared with the available experimental data in

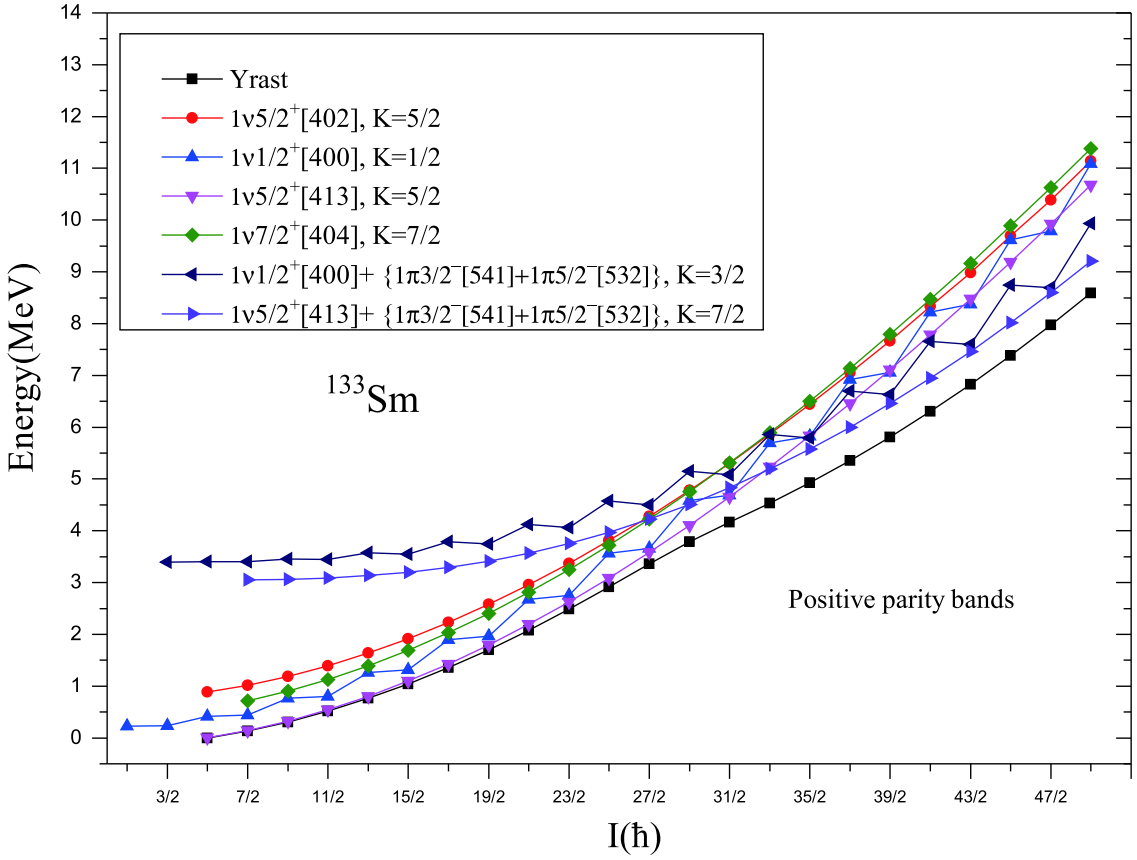

Fig. 2. (color online) Band diagram for positive parity bands for ^{133}Sm. Only low-lying and significant bands are taken.

Fig. 4. The calculated $\mathcal{J}^{(1)}$ values show back bending around I=29/2, 31/2 at rotational frequencies 0.430 and 0.400 MeV for bands 1 and 2, respectively. It is understood that in the spin range where the onset of back-bending takes place, it should be marked by the crossing of ground state band by the other bands and from the band diagram (Fig. 2), it can be seen that around spin $31/2^+$, $(h_{11/2})^2$ proton crossing takes place. Experimentally, it is also observed [4] that there is tentative evidence for the $(h_{11/2})^2$ proton crossing at a frequency $(\hbar\omega)$~0.35 MeV in bands 1 and 2, which is close to the calculated back-bending in $\mathcal{J}^{(1)}$ values around $\hbar\omega$~0.400-0.430 MeV, thereby predicting alignment of a pair of protons in $(h_{11/2})^2$ orbital. Thus, back-bending in moment of inertia, observed in the rotational spectra of deformed nuclei, carries important information on the interplay between the ground band and bands with alignment of a pair of quasi-particles.

3.1.2 Coupled bands 3 and 4

From the Fig. 2, it is seen that 1-qp neutron band built on K=1/2 and having configuration $1\nu 1/2^+[400]$ $(2d_{3/2})$ is the first excited positive parity band. Experimentally, first excited positive parity band is observed to be built upon Nilsson orbital $[411]1/2^+(d_{3/2})$ [4,28]. The present calculations have well reproduced the band head spin and configuration of this band. The present calculations show proximity of this excited band built on K=1/2 with the ground state band built on K=5/2 and both these bands are taken over by 3-qp bands having one neutron coupled to two $h_{11/2}$ protons at spin $33/2^+$ as can be seen in the Fig. 2. After band crossing, the first excited positive parity states are predicted to arise from the superposition of two 1-qp neutron bands having configurations $1\nu 5/2^+[413](2d_{5/2})$ and $1\nu 1/2^+[400](2d_{3/2})$. The band head energy of excited positive parity bands is not confirmed experimentally. However, the present calculations predict the band head energy of band 3 as 0.226 MeV with respect to positive parity yrast band 1. As the band head energies of these bands are not confirmed experimentally, the band spectra of these bands are not plotted for comparison. For comparison with experimental data [4,28], the transition energies $E(I)$-$E(I$-2) and $E(I)$-$E(I$-1) of bands 3 and 4 are plotted in Fig. 5. From this figure, it can be seen that $E2$ transition energies are reasonably reproduced at the lower spins for both bands 3 and 4. However, there is decrease in calculated $E2$ transitions around the spins $29/2^+$ and $35/2^+$, while as experimental values show no decrease in $E2$ transitions. The decrease in calculated $E2$ transitions at higher spins may be due to the crossing of 1-qp excited positive parity band by 3-qp

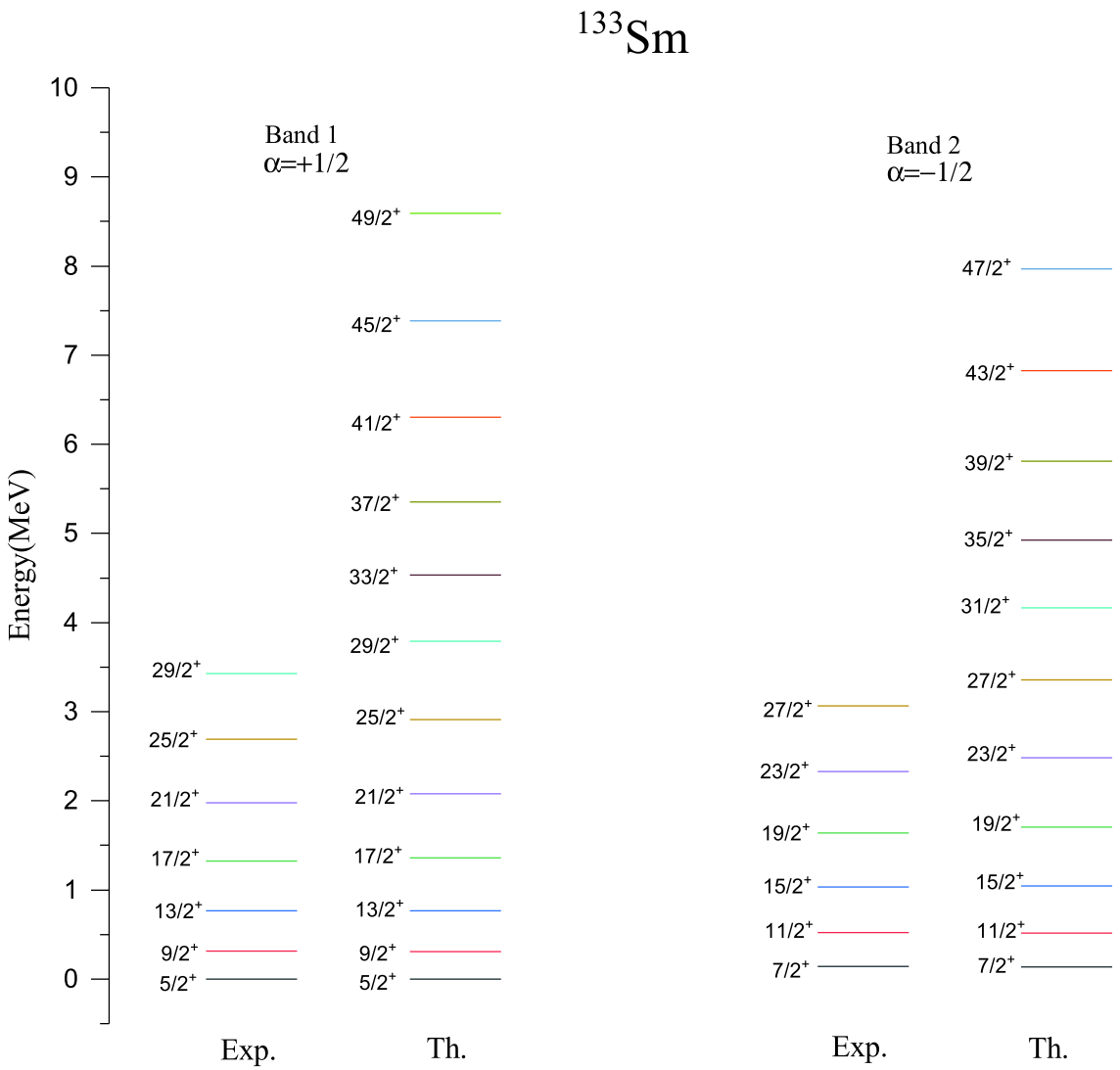

Fig. 3. (color online) Comparison of theoretical (Th.) energy levels with the available experimental (Exp.) data [28] for positive parity bands of ^{133}Sm.

bands. It is worthwhile to mention here that staggering in dipole transition energies $M1$ connecting bands 3 and 4 is well reproduced by the present calculations as shown in Fig. 5.

3.1.2.1 Kinetic moment of inertia of bands 3 and 4

The comparison of calculated kinetic moment of inertia $\mathcal{J}^{(1)}$ versus ω with the experimental ones for positive parity bands 3 and 4 is presented in Fig. 4. The calculated and experimental $\mathcal{J}^{(1)}$ values show the phenomenon of staggering in these bands due to the low value, K=1/2 of the band. The experimental band 3 (α=+1/2), shows an alignment around spin I=33/2 at $\hbar\omega$~0.347 MeV (also mentioned in Ref. [4]), whereas band 4 shows no alignment). The calculated results on $\mathcal{J}^{(1)}$ and ω show the phenomenon of back bending in band 3, around spin I=29/2 at $\hbar\omega$~0.288 MeV. Thus, the present calculations predict the band crossing and change in structure of bands 3 and 4 above spins I=29/2^{+} and 35/2^{+}, respectively.

3.1.3 Strongly coupled bands 5 and 6

Bands 5 and 6 have been assigned as being 1-qp structure built upon the neutron [523]7/2^{-}($h_{11/2}$) Nilsson orbital [4,28]. The experimental Routhians [4] show that both bands 5 and 6 have very little signature splitting up to the highest frequencies observed as would be expected from the high K assignments. The relative band head energies of negative parity bands 5,6 and 7 with respect to the ground state positive parity band are not confirmed experimentally. The present calculations predict the band head energy of band 5 as 0.179 MeV with respect to positive parity band 1. In Fig. 6, we plot the relevant low lying 1-qp and 3-qp negative parity bands in ^{133}Sm, along with their configurations. From the Fig. 6, it is seen that 1-qp neutron band built on K=7/2 and having configuration 1ν7/2^{-}[523] ($1h_{11/2}$) is lowest in energy out of all other negative parity bands, up to the spin I=39/2^{-}. The cal-

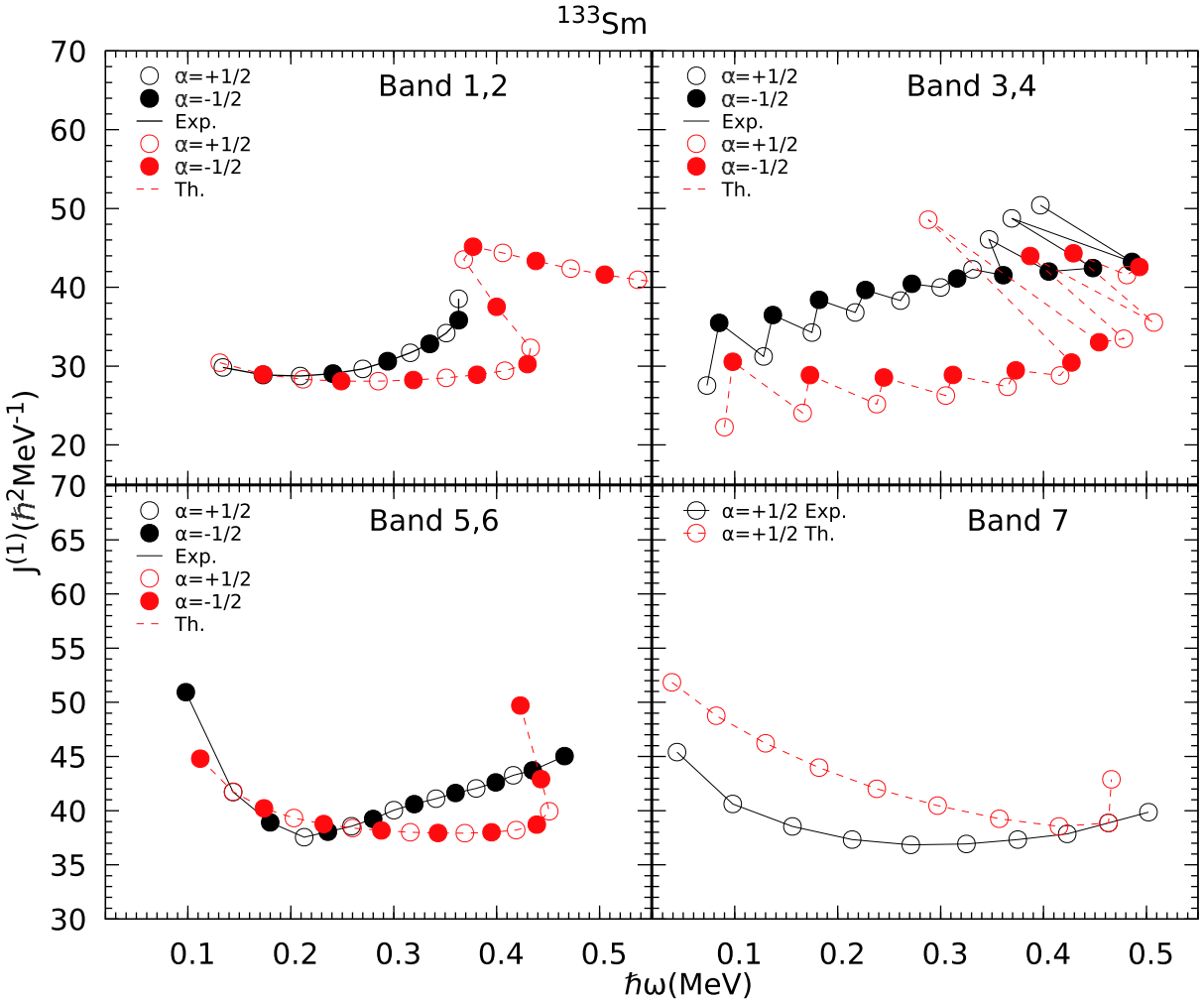

Fig. 4. (color online) Comparison of calculated and experimental kinetic moment of inertia $\mathcal{J}^{(1)}$, for bands 1-7 as a function of rotational frequency (ω) in ^{133}Sm.

culated results are very much consistent with the experimentally observed band head spin and configuration assigned to this band by the authors of Refs. [4,28]. Around spin $41/2^-$, this pure 1-qp neutron band is crossed by one 3-qp band consisting of one neutron $h_{11/2}$ coupled to two proton $h_{11/2}$ orbitals with $1\nu 7/2^-[523]+\{1\pi 3/2^-[541]+1\pi 5/2^-[532]\}$, K=5/2 as dominant configuration. Fig. 7 represents $E(I)$-$E(I$-2) transitions of bands 5 and 6 and dipole transitions $E(I)$-$E(I$-1), connecting these two bands. The calculated results show good agreement between theoretical and experimental transition energy values. There is decrease in calculated $E2$ and $M1$ transition energies around the spin $39/2^-$ which is due to the crossing of lowest negative parity band by the two 3-qp bands (as shown shown in Fig. 6).

3.1.3.1 Kinetic moment of inertia of bands 5 and 6

The comparison of calculated kinetic moment of inertia $\mathcal{J}^{(1)}$ versus ω with the experimental ones for negative parity bands 5 and 6 is presented in Fig. 4. The agreement between calculated and experimental curves at lower spins is good. The experimental curve of $\mathcal{J}^{(1)}$ versus ω show an increase around spin I=$25/2^-$ at $\hbar\omega$≈0.3 MeV. The calculated results show an increase in $\mathcal{J}^{(1)}$ around spin I=$39/2^-$, due to the crossing of 1-qp bands by 3-qp bands.

3.1.4 Decoupled band 7

Experimentally, this band 7 has been observed and assigned $[541]1/2^-$ ($h_{9/2}$) configuration by authors of Refs. [3,4,28]. The calculations of Ref. [4] suggest that this structure should have a quadrupole deformation β_2~0.33 which is nearly equal to the value of ε_2=0.33 used in the present study of bands 1-7. From the Fig. 6, the band built on K=$1/2^-$ and having configuration $1\nu 1/2^-[541]$ ($2f_{7/2}$) is an excited negative parity band. This band is very much consistent with the band head spin of the experimentally observed decoupled band 7. The relative band head energy of this band with respect to yrast negative parity band 5 is 0.444 MeV, that is not confirmed experimentally. In Fig. 8, the comparison of calculated and experimental [4,28] $E(I)$-$E(I$-2) transition energies is

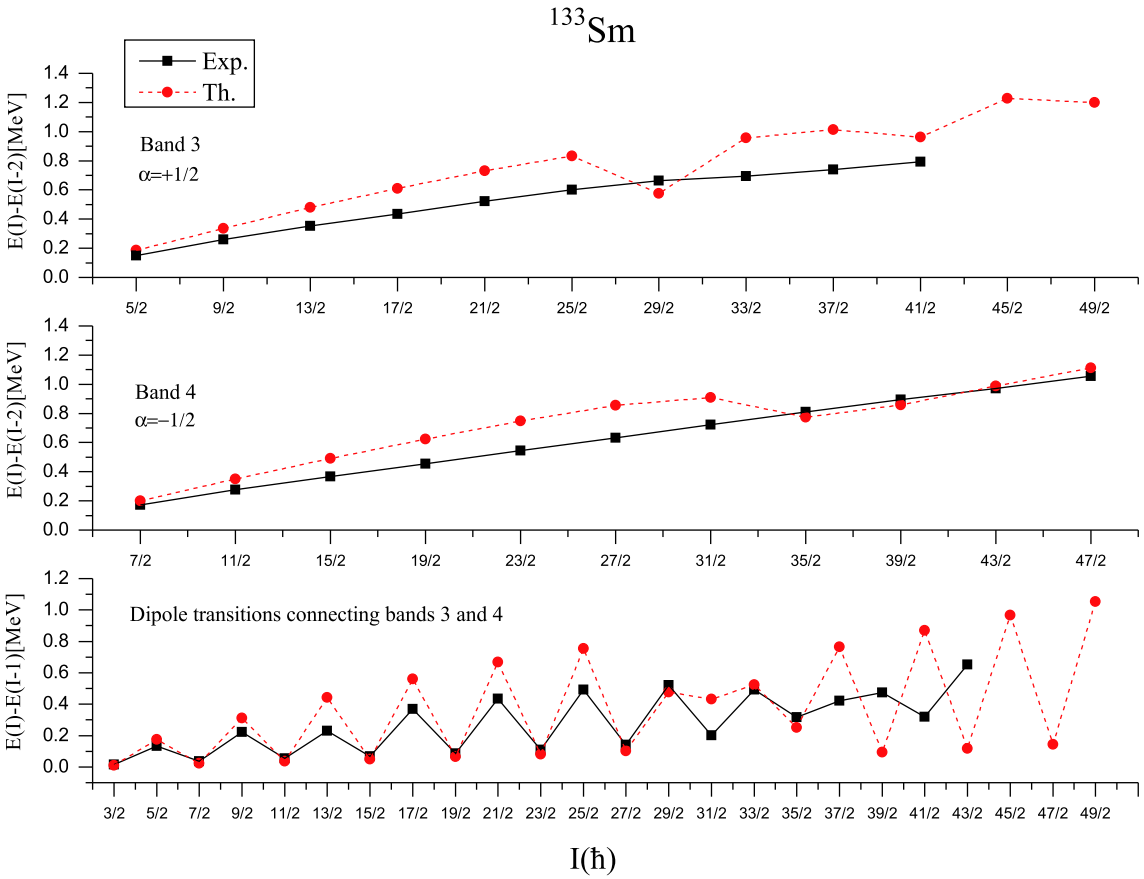

Fig. 5. (color online) Comparison of theoretical (Th.) and experimental (Exp.) [4,28] transition energy $E(I)$-$E(I$-2) versus angular momentum (I) for positive parity bands 3 and 4 and dipole transitions $E(I)$-$E(I$-1) versus angular momentum (I) connecting bands 3 and 4.

presented. From the figure, it can be seen that $E2$ transitions are very well reproduced up to I=37/2$^-$. The decrease in calculated $E2$ transitions at I=41/2 may be due to crossing by 3-qp bands.

3.1.4.1 Kinetic moment of inertia of band 7

The comparison of calculated kinetic moment of inertia $J^{(1)}$ versus ω with the experimental ones for negative parity band 7 is presented in Fig. 4. The calculated values reproduce the decreasing trend of experimental data up to I=37/2. The experimental curve of $J^{(1)}$ versus ω show an increase around spin I=29/2$^-$ at $\hbar\omega$~0.375 MeV. The calculated results show an increase in $J^{(1)}$ around spin I=37/2$^-$ at rotational frequency 0.45 MeV, due to the crossing of 1-qp bands by 3-qp bands.

3.2 ^{135}Sm

3.2.1 Discussion on band spectra

The review of experimental literature [5,26] reveals that the energies of band spectra of yrast positive and negative parity bands of ^{135}Sm are not confirmed experimentally yet and are tentative. In the present work, the band spectra have been obtained for ^{135}Sm with deformation parameters ε_2=0.275 and ε_4=0.070. The value of quadrupole deformation parameter ε_2 taken in the present calculation is consistent with the values of deformation parameters predicted for ^{135}Sm by the authors of Refs. [24,25]. However, the value of ε_4 has been increased from 0.033(0.020) to 0.070 to reproduce the experimental staggering in energies of yrast negative parity band 2. Fig. 9, shows the calculated energy levels for the positive parity 7/2$^+$ band represented by band 1 and negative parity 9/2$^-$ band represented by band 2, together with the experimental data [26]. As one can see, the data is reproduced rather well by the calculations up to the spin I= 19/2$^+$. In conformation with the suggestion of authors of Ref. [5], the 1-qp pure neutron configuration with K=7/2 from $g_{7/2}$ orbital is found to be lowest in energy defining the yrast sequence up to I=23/2$^+$. The difference between calculated and experimental value at the highest known spin I=39/2$^+$ (α=−1/2) of this band 1 is 0.532 MeV. This difference at the highest known spin I=29/2$^+$ (α=+1/2) of this band 1 is 0.731 MeV.

Now coming to the discussion of negative parity band spectra of ^{135}Sm, the calculated band spectra of 1-qp $h_{11/2}$ neutron orbital with K=9/2 represented as band 2 in Fig. 9 is a negative parity band of ^{135}Sm. The calculated energy levels corresponding to each angular momentum state of band 2 are in reasonable agreement with the tentative ex-

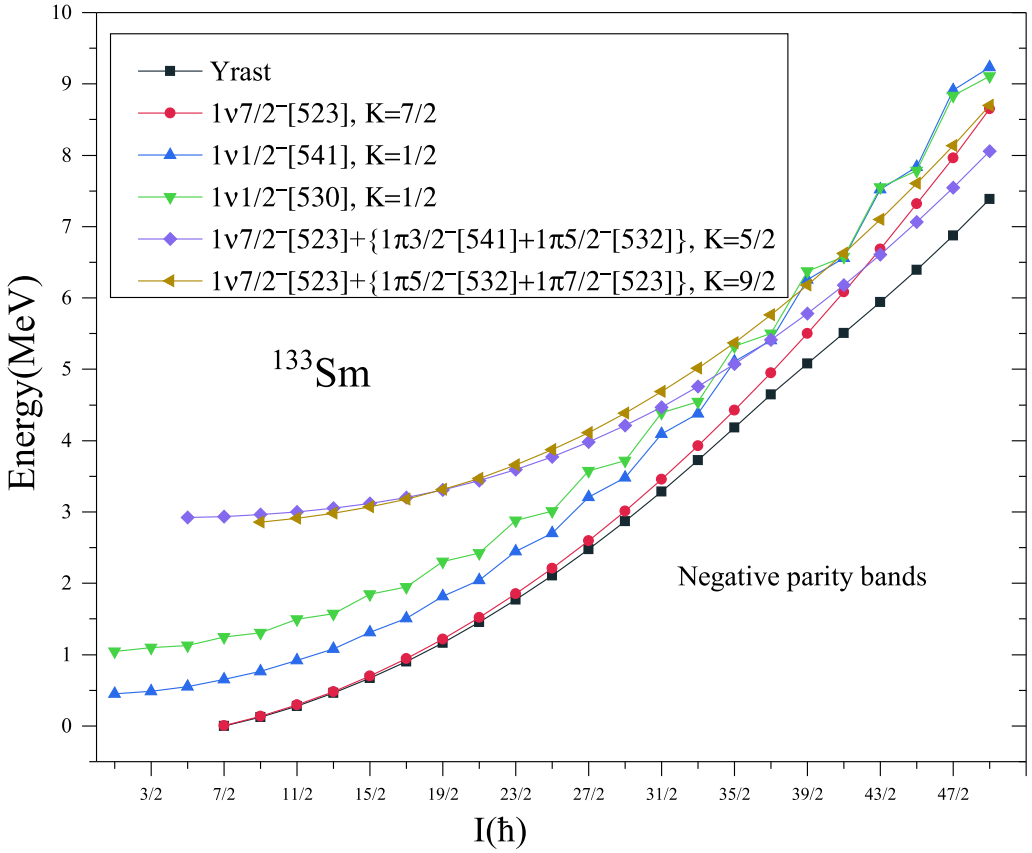

Fig. 6. (color online) Band diagram for negative parity bands for ^{133}Sm. Only low-lying and significant bands are taken.

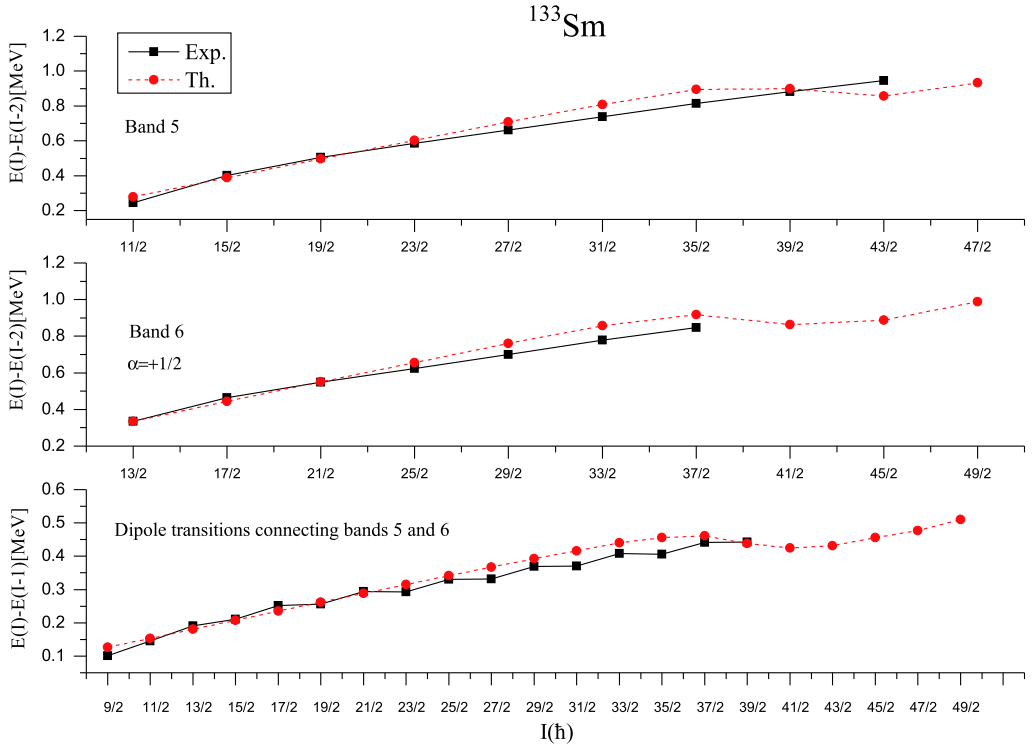

Fig. 7. (color online) Comparison of theoretical (Th.) and experimental (Exp.) [4,28] transition energy $E(I)$-$E(I$-2) versus angular momentum (I) for negative parity bands 5 and 6 and dipole transitions $E(I)$-$E(I$-1) versus angular momentum (I) connecting bands 5 and 6.

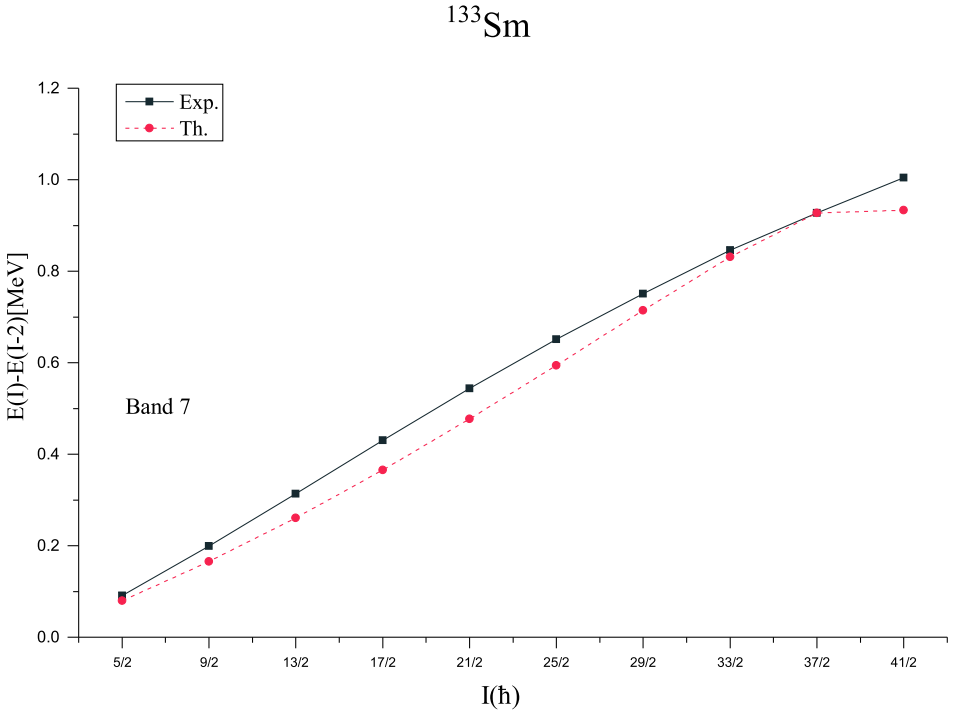

Fig. 8. (color online) Comparison of theoretical (Th.) and experimental (Exp.) [4,28] transition energy $E(I)$-$E(I$-2) versus angular momentum (I) of band 7.

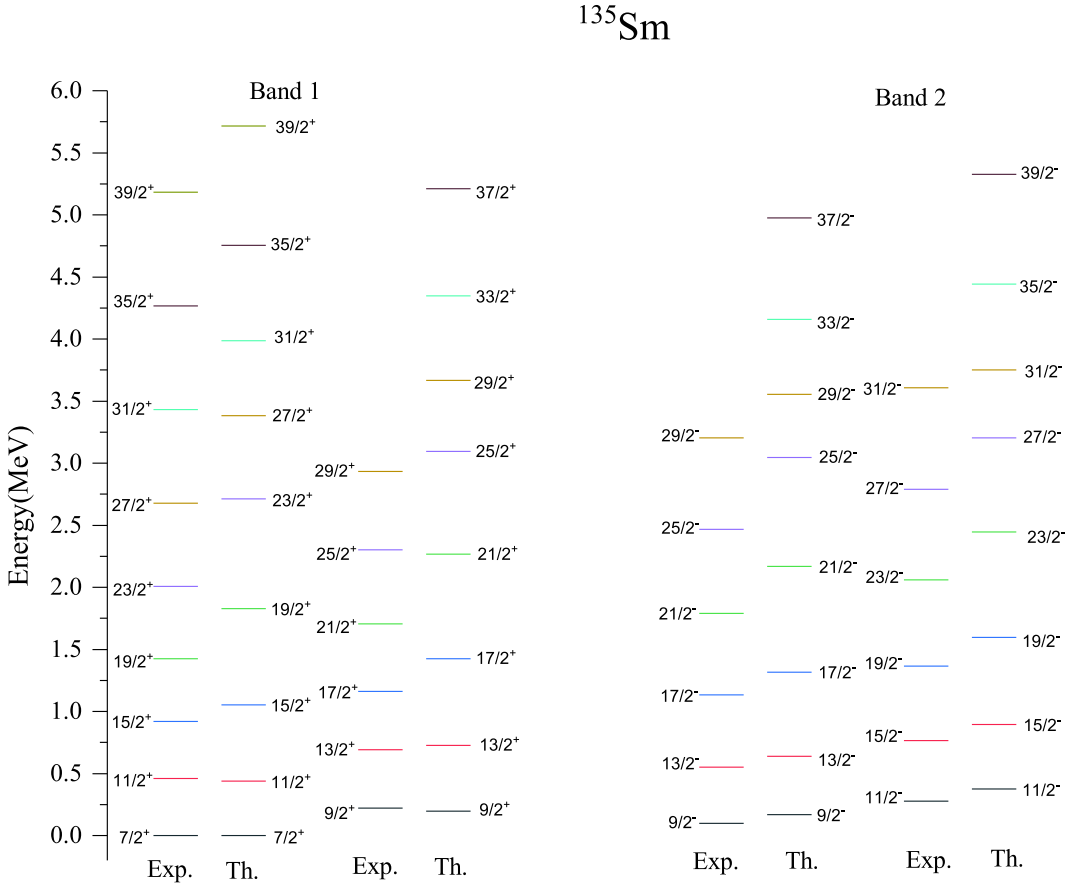

Fig. 9. (color online) Comparison of theoretical (Th.) energy levels with the available experimental (Exp.) data [26] for positive parity band 1 and negative parity band 2 of ^{135}Sm.

perimental data of Ref. [26]. The approximate band head energy of band 2 at band head spin I=9/2$^-$ is 0.10 MeV, whereas the present calculations predict it as 0.17 MeV. The difference between calculated and tentative experimental values at the band head spin I=9/2$^-$ is 0.07 MeV and this difference at the highest known spin 31/2$^-$ is 0.145 MeV. As mentioned in the preceding discussion, the level energies of these bands are tentative, therefore, one cannot comment on the level of agreement precisely. Further, the transition energies of bands 1 and 2 of ^{135}Sm are confirmed experimentally, therefore these energies are compared with experimental data in Figs. 10 and 11 for positive and negative parity bands 1 and 2, respectively. From these figures, it is observed that, $E(I)$-$E(I$-2) transition energies show reasonably good agreement with the experimental data at low spins and show a decrease at spins I=27/2 and 29/2 in positive and negative parity bands, respectively. However, the $E(I)$-$E(I$-1) transition energies show good agreement with the available experimental data of both bands 1 and 2.

3.2.2 Discussion on band diagrams

In Fig. 12, we plot the relevant 1-qp and 3-qp positive parity bands in ^{135}Sm, along with their configurations. From the Fig. 12, it is seen that 1-qp neutron band built on K=7/2 and having configuration $1v7/2^+[404](1g_{7/2})$ is lowest in energy up to the spin I=25/2$^+$. This observation is consistent with the band head spin and configuration assigned to it by the authors of Ref. [5]. The yrast states of this band arise from $1v7/2^+[404](1g_{7/2})$ configuration up to I=23/2. However, at the spin 27/2$^+$ band crossing occurs and 3-qp bands consisting of one neutron coupled to a pair of protons and having configurations $1v7/2^+[404]+\{1\pi1/2^-[550]+1\pi5/2^-[532]\}$, K=13/2; $1v7/2^+[404]+\{1\pi3/2^-[541]+1\pi5/2^-[532]\}$, K=9/2 and $1v5/2^+[413]+\{1\pi3/2^-[541]+1\pi5/2^-[532]\}$, K=7/2, crosses the 1-qp, K=7/2 band. This band crossing causes a significant change in the yrast structure of ^{135}Sm.

The band diagram for negative parity states is shown in Fig. 13, in which only important 1-qp and 3-qp bands along with their configurations are shown. The dominant structure of the lowest negative parity band is K=9/2 state of the neutron $1h_{11/2}$ orbital up to the spin 13/2$^-$. This is consistent with the band head spin and configuration assigned to this band by the authors of Ref. [26]. From the spin 15/2$^-$ to 23/2$^-$, the lowest energy states are formed due to the contribution of different 1-qp bands having configurations $1v7/2^-[523](1h_{11/2})$, $1v9/2^-[514](1h_{11/2})$ and $1v1/2^-[541](2f_{7/2})$. It may be because of this configuration mixing at low spins, the calculated results show staggering in energies, which increases in magnitude with increase in spin up to the spin I=25/2$^-$. This staggering in calculated ΔI=1 transition energies are well supported by

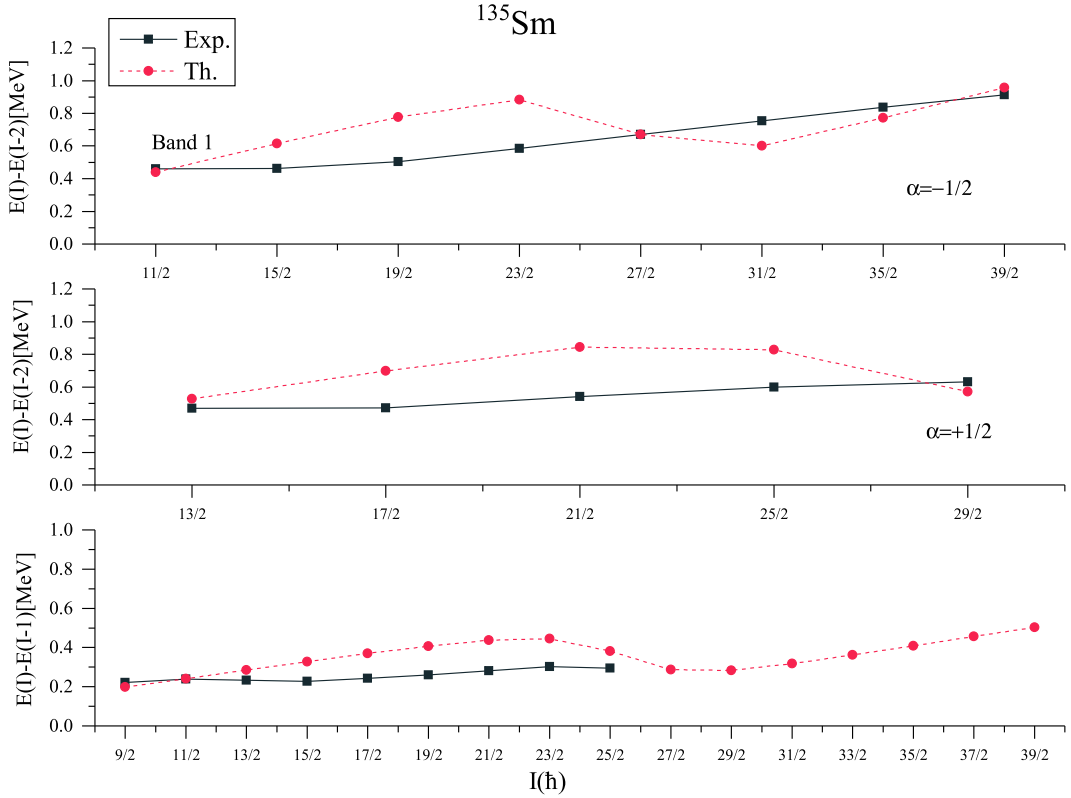

Fig. 10. (color online) Comparison of theoretical (Th.) and experimental (Exp.) [26] transition energy $E(I)$-$E(I$-2) and $E(I)$-$E(I$-1) of band 1 versus spin angular momentum (I) of ^{135}Sm.

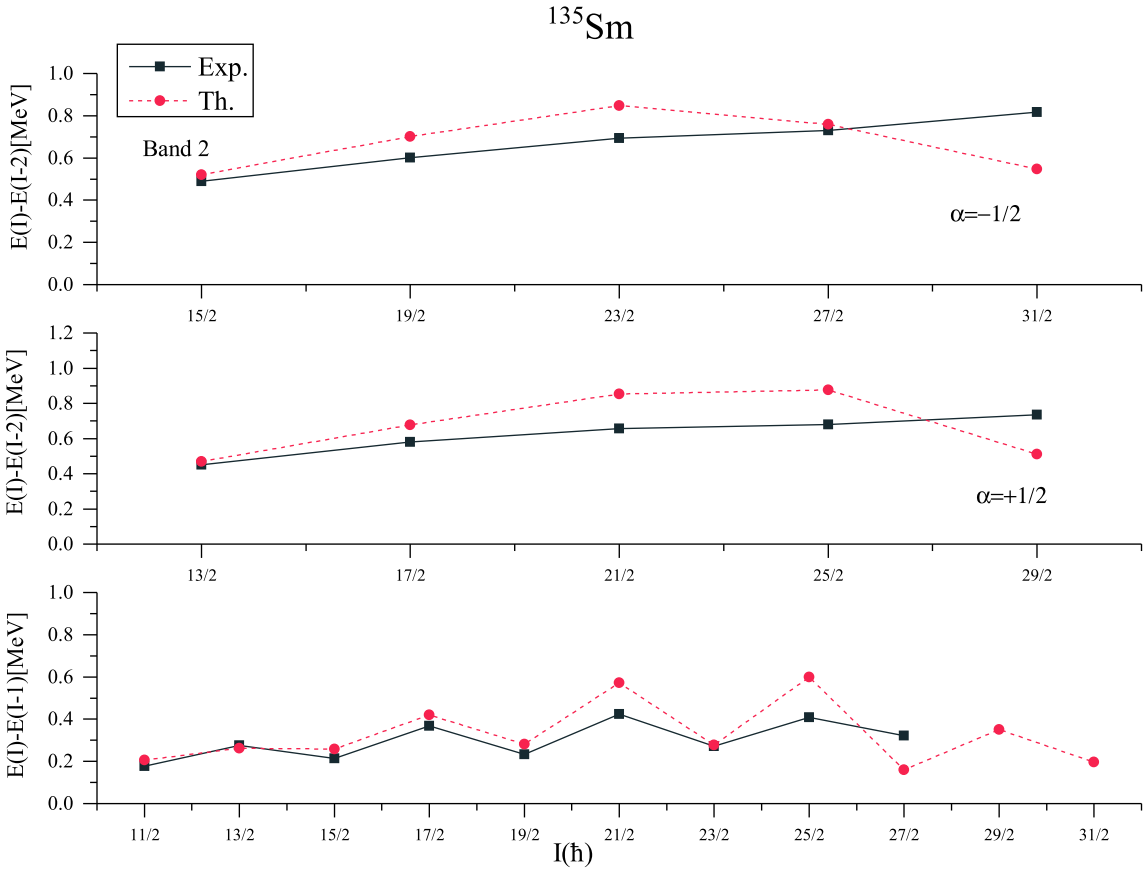

Fig. 11. (color online) Comparison of theoretical (Th.) and experimental (Exp.) [26] transition energy $E(I)$-$E(I$-2) and $E(I)$-$E(I$-1) versus spin angular momentum (I) for band 2 ($\alpha = \mp 1/2$).

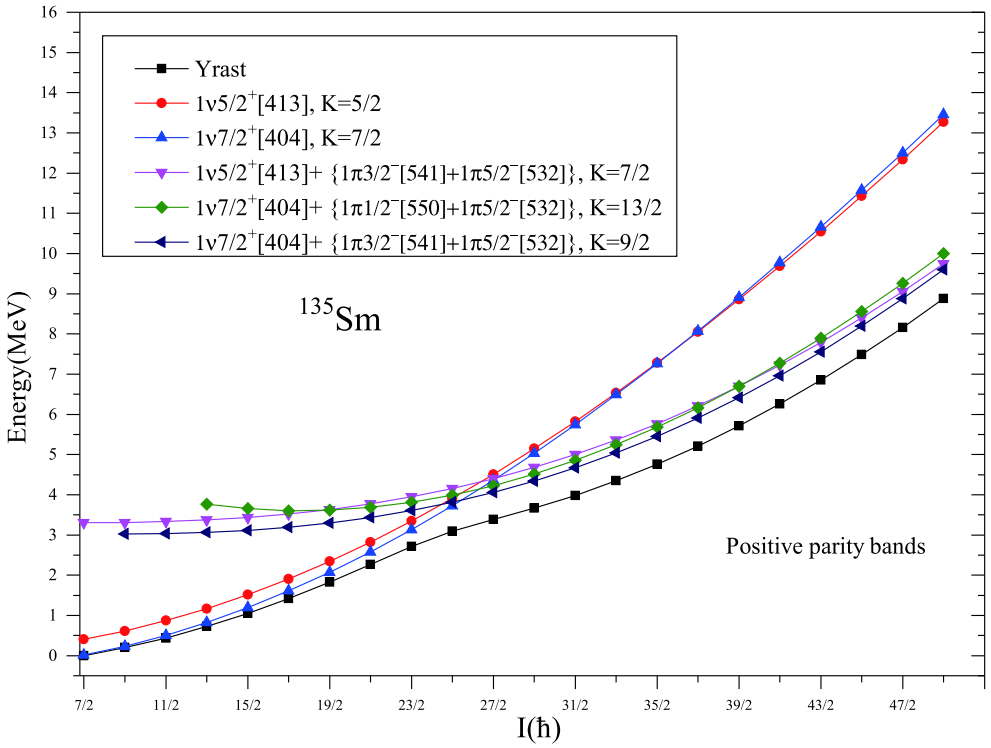

Fig. 12. (color online) Band diagram for positive parity bands for ^{135}Sm. Only low-lying and significant bands are taken.

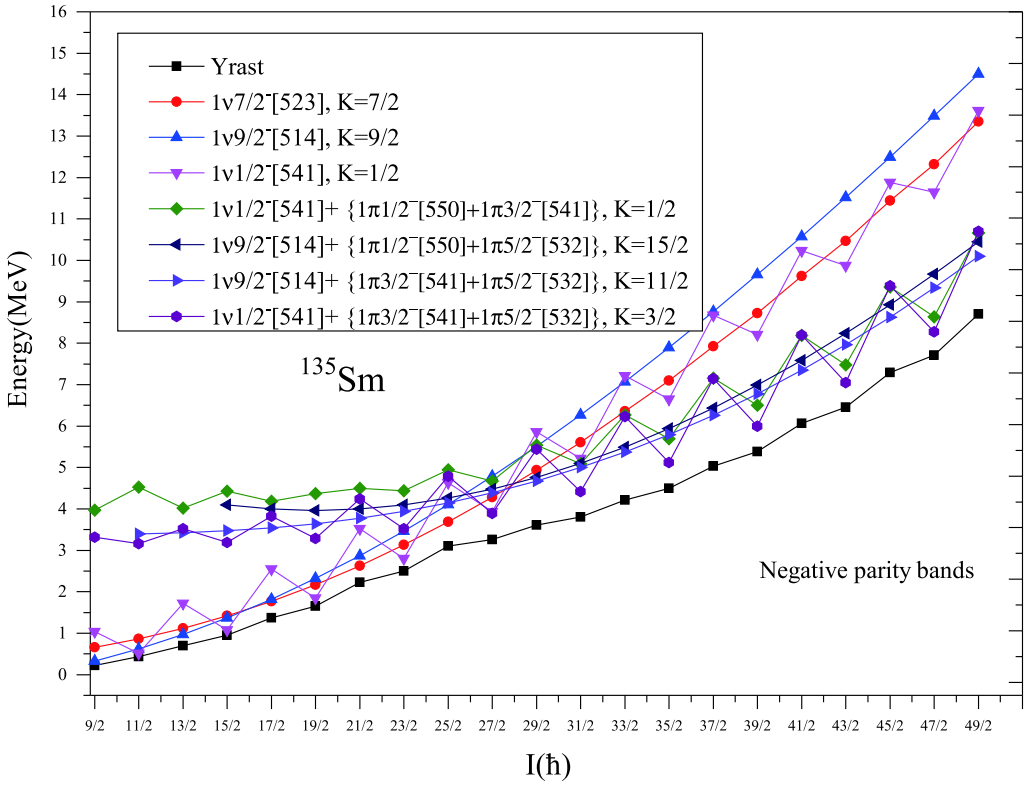

Fig. 13. (color online) Band diagram for negative parity bands for ^{135}Sm. Only low-lying and significant bands are taken.

the experimentally observed staggering in ΔI=1 transition energies (shown in Fig. 11). The staggering pattern is more clear from the plots of kinetic moment of inertia $\mathcal{J}^{(1)}$ versus ω, presented in Fig. 14 for band 2.

3.2.3 Kinetic moment of inertia of bands 1 and 2

The comparison of calculated kinetic moment of inertia $\mathcal{J}^{(1)}$ versus ω with the experimental ones for yrast bands 1 and 2 of ^{135}Sm, is presented in Fig. 14. The calculated curve for band 1 shows a large increase in $\mathcal{J}^{(1)}$ values at spin I=27/2 at rotational frequency $\hbar\omega$~0.34 MeV thereby, predicting the phenomenon of backbending in the vicinity of the region of crossing of 1-qp bands by 3-qp bands. However, the change in experimental $\mathcal{J}^{(1)}$ curve observed in experimental values around spin I=25/2, at $\hbar\omega$~0.30 is less pronounced as compared to calculated results.

Now, coming to band 2, the comparison of calculated and experimental $\mathcal{J}^{(1)}$ versus ω plots, presented in Fig. 14, for band 2, show the staggering pattern clearly. The calculated results reproduce the experimental zigzag pattern, nicely. However, the calculated values of $\mathcal{J}^{(1)}$ show a large increase in $\mathcal{J}^{(1)}$ at I=25/2 at $\hbar\omega$~0.28 MeV due to the crossing of 3-qp bands. Thus, the calculated results predict a sharp change in $\mathcal{J}^{(1)}$ in yrast positive and negative parity bands 1 and 2 of ^{135}Sm at higher spins around the band crossing region due to the large crossing angle between the 1-qp and 3-qp bands.

3.3 ^{137}Sm

3.3.1 Discussion on band spectra

In ^{137}Sm, the experimental band spectra and band head energies of yrast negative and positive parity bands are confirmed experimentally [6,7,27]. Calculations are performed for ^{137}Sm with the deformation parameters ε_2=0.20 and ε_4=0.04 for the yrast negative and positive parity bands 1 and 2, of ^{137}Sm. These values of deformation parameters are the same as predicted for ^{137}Sm by the authors of Refs. [24,25]. Figure 15 shows the calculated energy levels for yrast I=9/2$^-$ negative and I=7/2$^+$ positive parity bands together with the experimental data of Ref. [27]. As one can see from the Fig. 15, the calculated experimental data of negative parity band 1 are reproduced very well by the present calculations. The difference between the experimental and calculated values at the highest known spin 43/2$^-$ is only 0.044 MeV. Now coming to the discussion on energy level spectra of the positive parity band built on band head spin I^π =7/2$^+$ and represented by band 2 in the Fig. 15, the energies of the experimental and calculated band head spins are almost same. It means the experimental energy of the band head spin 7/2$^+$ of this positive parity band is exactly reproduced. The difference between experimental and calculated values at the highest known spin 37/2$^+$ of band 2 is 0.429 MeV.

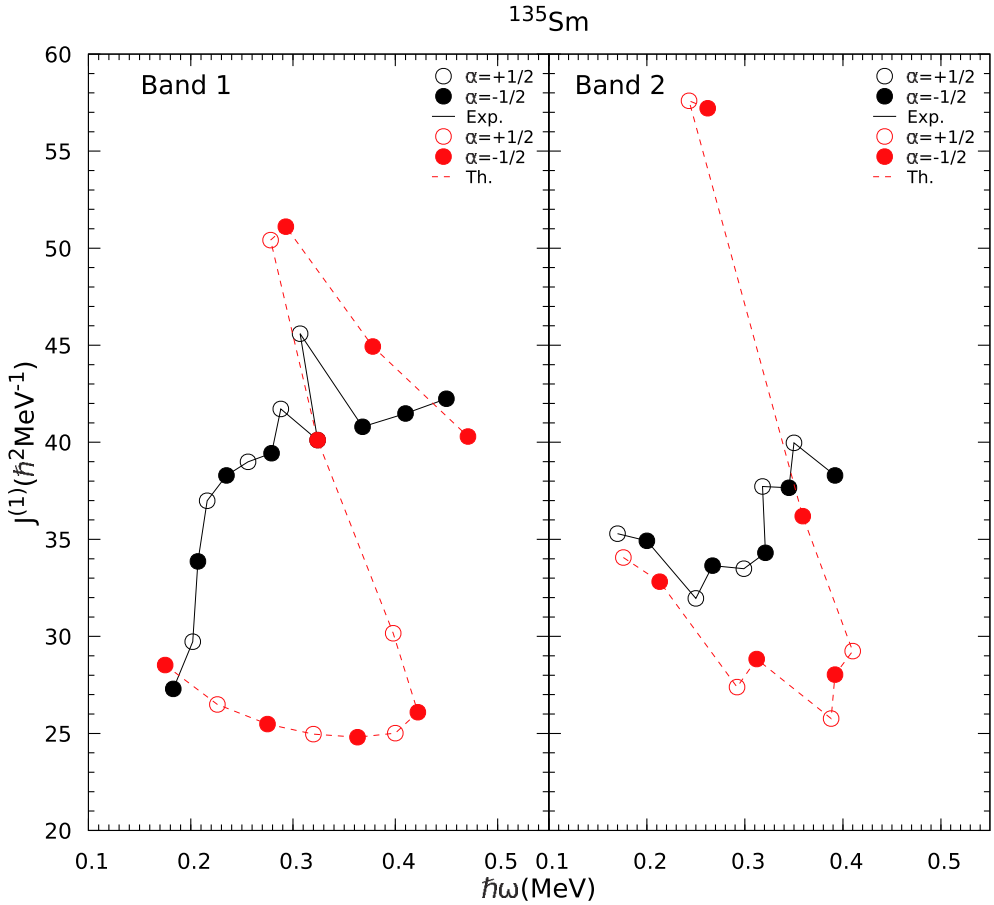

Fig. 14. (color online) Comparison of calculated and experimental kinetic moment of inertia $\mathcal{J}^{(1)}$, for bands 1,2 as a function of rotational frequency (ω) in ^{135}Sm.

3.3.2 Discussion on band diagrams

Figure 16 shows relevant 1-qp and 3-qp bands of negative parity along with their configurations for ^{137}Sm. From the figure, it is evident that the dominant structure of yrast band up to the spin $15/2^-$ is K=9/2 state of neutron $h_{11/2}$ orbital, which is consistent with the band head spin and configuration observed for this band by the authors of Refs. [6,7,27]. At the spin I=$17/2^-$, another 1-qp neutron $2f_{7/2}$ band interacts with this 1-qp $h_{11/2}$ band and energy states of the yrast band from the spin I=$19/2^-$ to I=$23/2^-$ are predominantly arising from K=1/2 state of $1\nu 2f_{7/2}$ orbital. Around the spin I=$25/2^-$, the 1-qp neutron bands are crossed by two 3-qp bands consisting of single neutron coupled to a pair of protons with configurations $1\nu 9/2^-[514]+\{1\pi 1/2^-[550]+1\pi 3/2^-[541]\}$, K=11/2 and $1\nu 9/2^-[514]+\{1\pi 1/2^-[550]+1\pi 5/2^-[532]\}$, K=15/2. This band crossing causes a significant change in the yrast structure of ^{137}Sm and the yrast states of negative parity band above I=23/2 are predicted to arise from the superposition of these two 3-qp bands.

Figure 17 represents the band diagram for positive parity bands of ^{137}Sm. From this figure, it can be seen that the 1-qp neutron band from K=7/2 state of neutron orbital $g_{7/2}$ is lowest in energy from all the other positive parity bands. This lowest energy band of positive parity goes monotonically up to the spin I=$21/2^+$. The authors of Ref. [8] proposed this band to originate from the K=1/2 state of neutron $d_{3/2}$ orbital. However, reasonably good agreement with the experimental energies for whole of this band support it to arise from the predicted configuration $1\nu 7/2^+[404](1g_{7/2})$ for this band. Further, at the spin I=$23/2^+$, band crossing by multiple 3-qp bands causes a significant change in the energy states of the lowest positive parity states. It can be predicted that after the band crossing the lowest positive parity states has a composite structure and are predicted to arise from the superposition of multi 3-qp bands whose configurations are shown in the Fig. 17.

3.3.3 Discussion on Kinetic moment of Inertia

The experimental and calculated $\mathcal{J}^{(1)}$ versus ω plots for ^{137}Sm are displayed in Fig. 18. From this figure, it is observed that for negative parity band 1, both the experimental and calculated results show the phenomenon of backbending at the same spin I=$25/2^-$ and at rotational frequencies $\hbar\omega$=0.34 and 0.366, respectively. The crossing frequencies predicted by the present calculations are

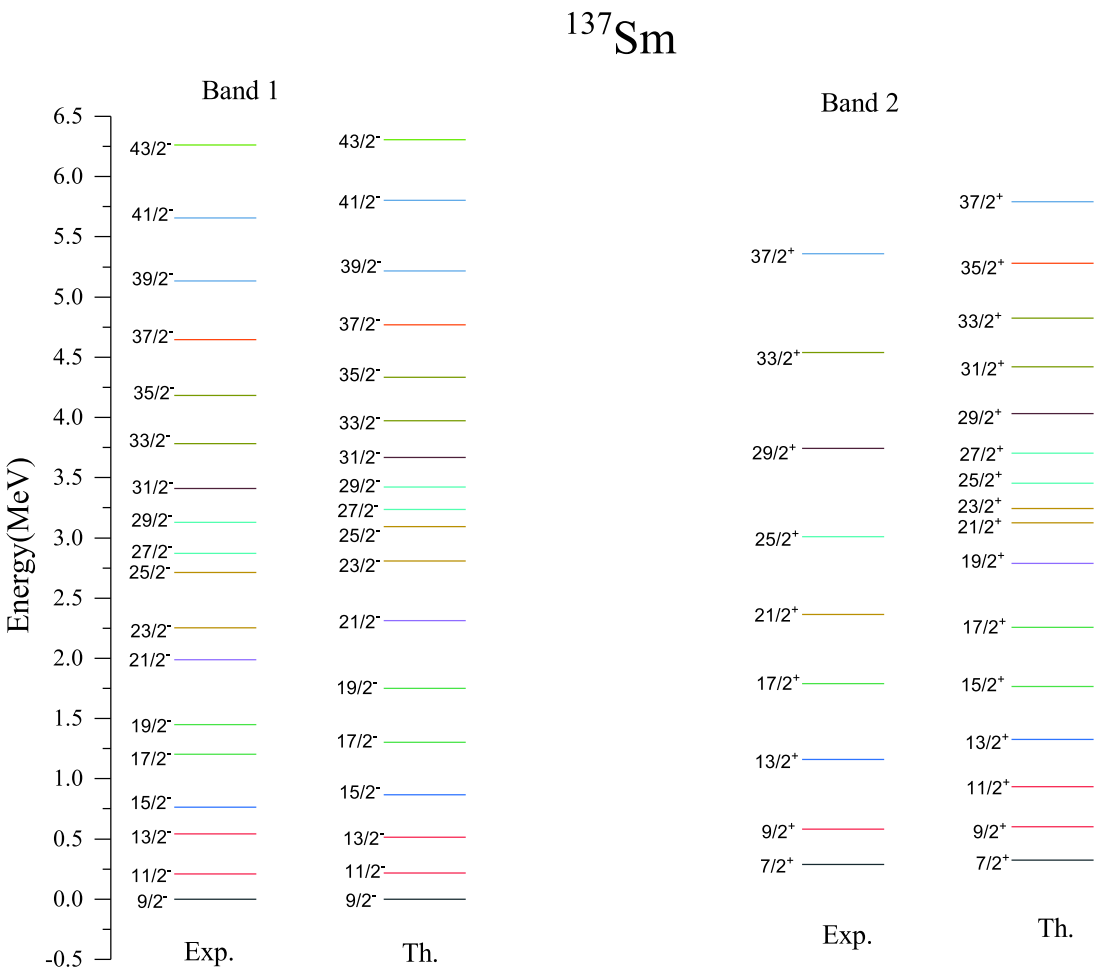

Fig. 15. (color online) Comparison of theoretical (Th.) energy levels with the available experimental (Exp.) data [27] for negative parity band 1 and positive parity band 2 of ^{137}Sm.

consistent with those given in Ref. [6]. This phenomenon of backbending occurs at the spin around which 1-qp neutron bands are crossed by 3-qp ($1\nu+2\pi$) bands as seen in Fig. 16 and it may be due to the alignment of a pair of protons in the $\pi(h_{11/2})^2$ orbitals. However, the staggering observed at low spins is not reproduced by the present calculation.

Similarly, the $\mathcal{J}^{(1)}$ versus ω, plots of positive parity band 2, presented in the same figure, show the phenomenon of backbending in the experimental and calculated results at the same spin $I=21/2^+$ and at rotational frequencies $\hbar\omega$=0.273 and 0.411, respectively and it is due to the crossing of 1-qp neutron band by 3-qp ($1\nu+2\pi$) bands as seen in Fig. 17. Thus, the phenomenon of backbending in the yrast negative and positive parity bands of ^{137}Sm, arises due to the alignment of a pair of protons in the down slopping K- components of $\pi(h_{11/2})^2$ orbitals.

4 Electromagnetic quantities

The energy of electromagnetic radiation field can be described mathematically in terms of a multipole moment expansion. The terms correspond to $2n$ - pole and the lowest terms are n=0 (monopole), n=1 (dipole), n=2 (quadrupole), n=3 (octupole), n=4 (hexadecapole) and so on. The electric quadrupole transition probability $B(E2)$ of a nucleus is sensitive to nuclear charge distribution and collective effects such as deformation. The magnetic dipole transition probability $B(M1)$ are sensitive to nuclear magnetic moments and single particle properties. Experimentally, it is difficult to obtain absolute $B(E2)$ and $B(M1)$ values through measurements of mean life times of nuclear states. In contrast, it is relatively easy to extract the ratio $B(M1)/B(E2)$, knowing just γ-ray energies and intensities. The $B(M1)/B(E2)$ values are sensitively dependent on the single particle angular momentum states occupied by the valence protons and neutrons. These are directly linked to the wave functions of the system and their prediction poses an important test for nuclear structure models. It is therefore important to calculate these quantities for rotational bands of odd mass neutron deficient Sm isotopes.

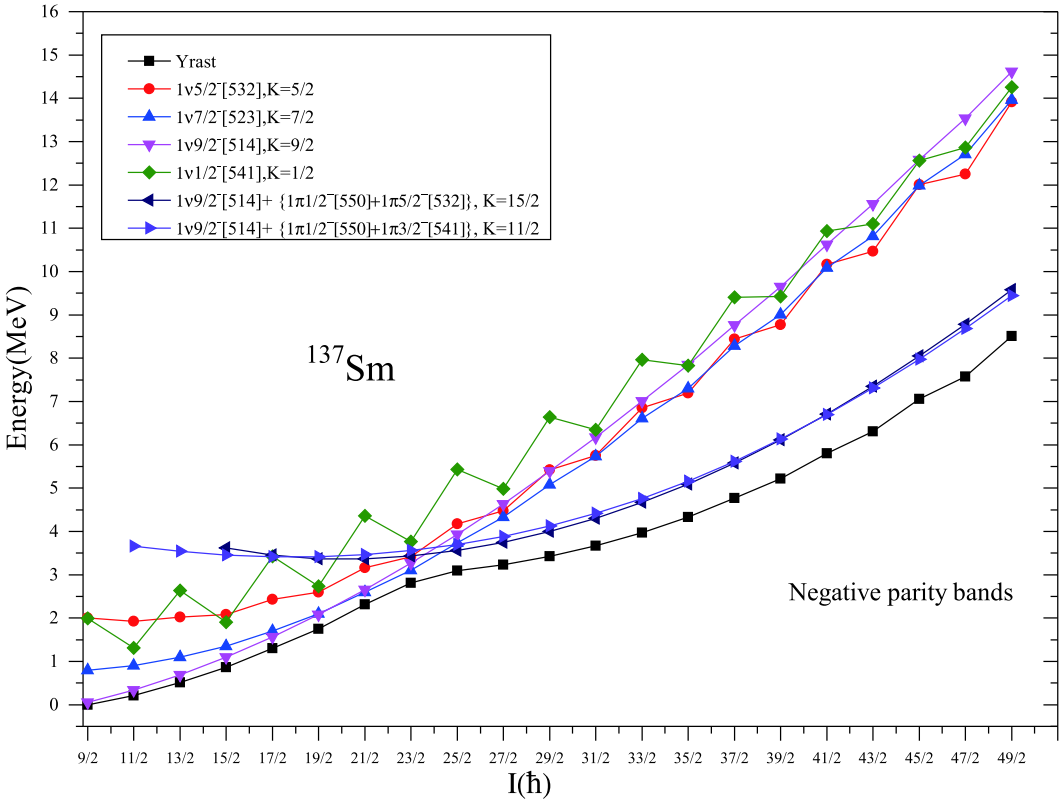

Fig. 16. (color online) Band diagram for negative parity bands for ^{137}Sm. Only low-lying and significant bands are taken.

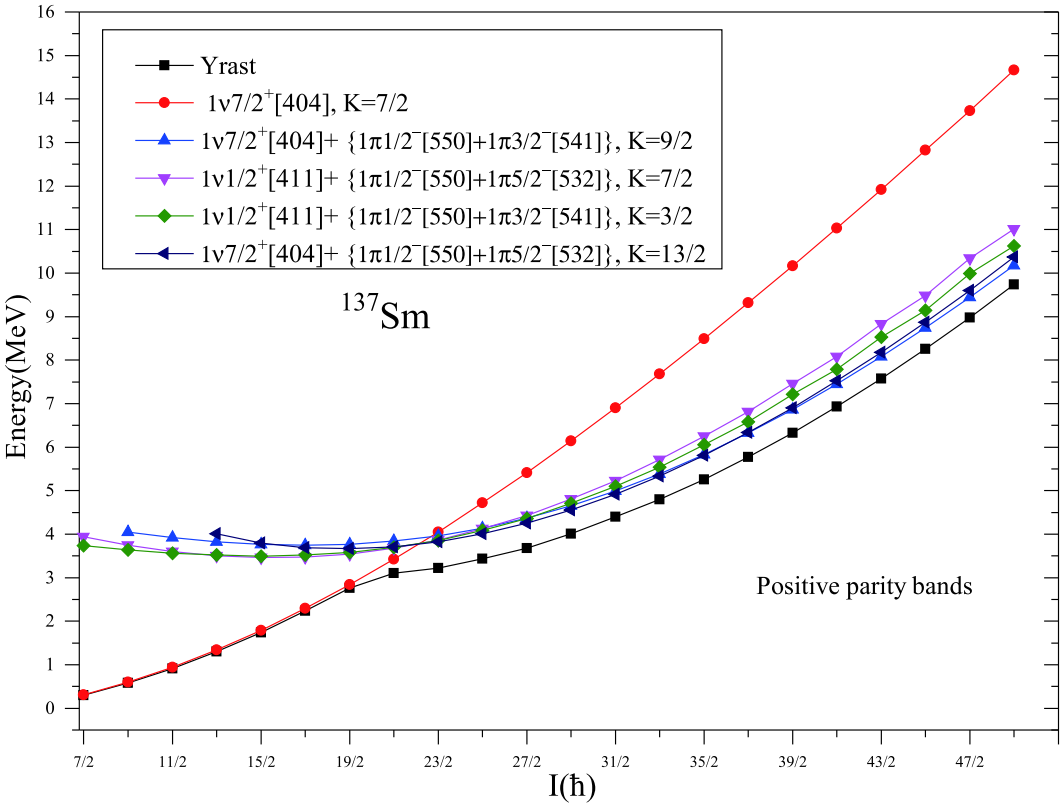

Fig. 17. (color online) Band diagram for positive parity bands for ^{137}Sm. Only low-lying and significant bands are taken.

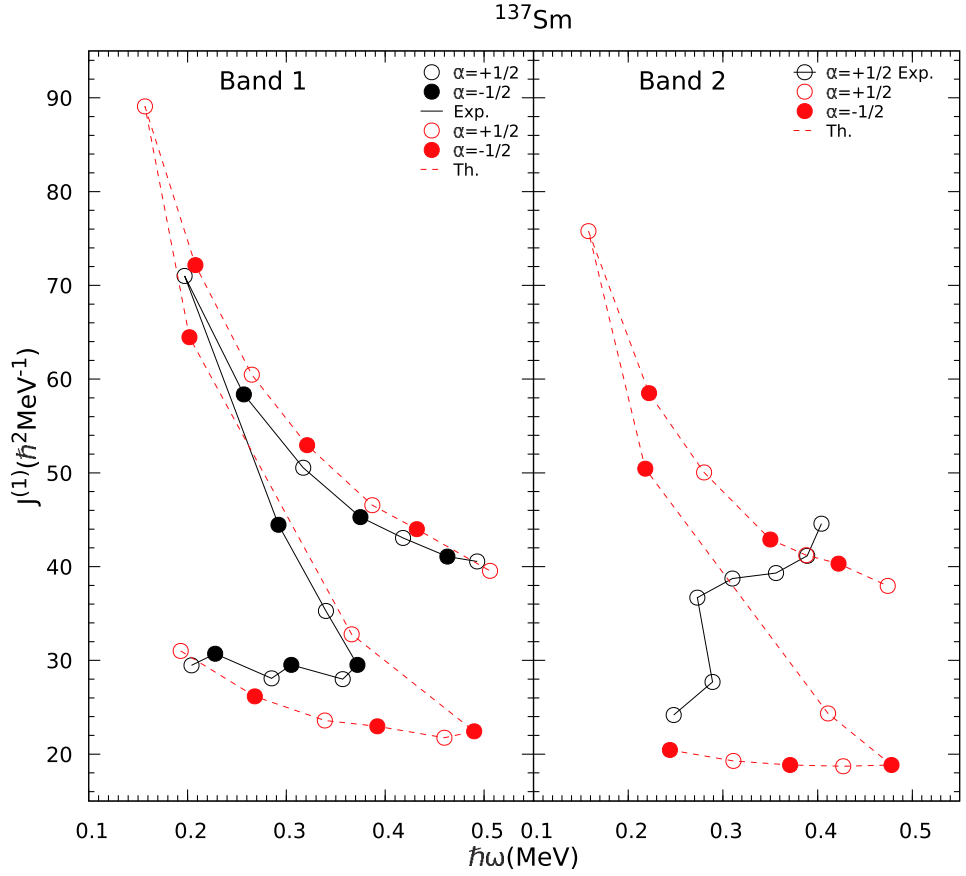

Fig. 18. (color online) Comparison of calculated and experimental kinetic moment of inertia $J^{(1)}$, for bands 1,2 as a function of rotational frequency (ω) in ^{137}Sm.

The calculation of electromagnetic transition probabilities [30] are important for the reliability of the wave functions generated by Eq. (1). The reduced electric quadrupole transition probability $B(E2)$ from an initial state I_i =I to a final state I_f=I-2 is given by

$$B\left(E2, I_i \to I_f\right) = \frac{e^2}{(2I_i+1)}\left|\left\langle \sigma_f, I_f \left\| \hat{Q}_2 \right\| \sigma_i, I_i \right\rangle\right|^2,$$

where the operator $\hat{Q}_2$ is related to the quadrupole operator. In the present calculations, the proton and neutron effective charges are calculated as $e_\pi = e[1+(e_{\rm eff})]$ and $e_\nu = e(e_{\rm eff})$ with $e_{\rm eff} = 0.5$ for all Sm nuclei studied in this paper.

The $B(M1)$ transition probability from an initial state I_i = I to a final state I_f= I-1 is calculated by using the relation

$$B\left(M1, I_i \to I_f\right) = \frac{\mu_N^2}{2I_i+1}\left|\left\langle \sigma_f, I_f \left\| \hat{M}_1 \right\| \sigma_i, I_i \right\rangle\right|^2$$

where the magnetic dipole operator is defined as $\hat{M}_1^\tau = g_l^\tau \hat{J}^\tau + \left(g_s^\tau - g_l^\tau\right)\hat{s}^\tau$. Here τ is either π or ν and g_l and g_s are the orbital and spin gyromagnetic factors, respectively. In the present calculations, the free values of g_l are taken and for g_s the free values are damped by a 0.75 factor

$$g_l^\pi = 1 \quad g_s^\pi = 5.59 \times 0.75 \quad g_l^\nu = 0 \quad g_s^\nu = -3.826 \times 0.75$$

4.1 Results and discussion on transition strength ($B(M1)/B(E2)$) ratios of ^{133}Sm

The experimental data on $B(E2)$ and $B(M1)$ transition probabilities is not available for $^{133\text{-}137}$Sm isotopes, but the experimental data [4,6,8] on $B(M1)/B(E2)$ ratios is available for low spin states of ^{133,137}Sm. Therefore, $B(M1)/B(E2)$ ratios are presented in Table 2 for comparison with the available experimental data and the results are discussed in the following subsections.

4.1.1 Positive parity bands 1 and 2

The experimental data on $B(M1)/B(E2)$ ratios is known up to spin I=17/2 only. The comparison of calculated $B(M1)/B(E2)$ ratios with the available experimental data [4] is represented in Table 2. The agreement between calculated transition strengths and available experimental values is good except at the angular momentum state $13/2^+$. The experimental data, show an increase in $B(M1)/B(E2)$ values as one moves from spin I=9/2 to 13/2, and a decrease from I=13/2 to 17/2. The calculated results predict a decreasing trend with spin up to the band crossing spin I=33/2, thereby, showing a change in the

Table 2. Comparison of calculated $B(M1)/B(E2)$ ratios with the available experimental data [4,6,8] for (a) ^{133}Sm, (b) ^{135}Sm and (c) ^{137}Sm.

Nucleus	Positive parity yrast bands 1 and 2			Negative parity yrast bands 5 and 6	
(a) ^{33}Sm	Spin (I)	$B(M1)/B(E2)$ $(\mu_n/eb)^2$		$B(M1)/B(E2)$ $(\mu_n/eb)^2$	
		Exp. [4]	Th.	Exp.	Th.
	9/2	0.766±0.251	0.936	–	–
	11/2	0.782±0.190	0.633	0.372±0.114	0.749
	13/2	0.827±0.159	0.530	0.300±0.200	0.487
	15/2	0.570±0.123	0.476	0.349±0.143	0.402
	17/2	0.452±0.092	0.441	0.306±0.200	0.360
	19/2		0.415		0.336
	21/2		0.394		0.319
	23/2		0.373		0.308
	25/2		0.353		0.297
	27/2		0.325		0.292
	29/2		0.278		0.279
	31/2		0.179		0.276
	33/2		0.098		0.255

Nucleus	Positive parity yrast band 1		
(b) ^{135}Sm	Spin (I)	$B(M1)/B(E2)$ $(\mu_n/eb)^2$	
		Exp.	Th.
	11/2	–	0.176
	13/2	–	0.124
	15/2	–	0.111
	17/2	–	0.109
	19/2	–	0.110
	21/2	–	0.111
	23/2	–	0.109
	25/2	–	0.092
	27/2	–	0.072
	29/2	–	0.175

Nucleus	Negative parity yrast band 1		
(c) ^{137}Sm	Spin (I)	$B(M1)/B(E2)$ $(\mu_n/eb)^2$	
		Exp.[6,8]	Th.
	13/2	$0.771^{+0.166}_{-0.115}$	1.184 ±0.089	0.990
	15/2	$1.00^{+0.176}_{-0.15}$	0.768±0.095	0.802
	17/2	$0.576^{+0.080}_{-0.086}$	0.663±0.053	0.677
	19/2	$1.944^{+0.164}_{-0.208}$	0.858	0.672
	21/2	$1.176^{+0.185}_{-0.176}$	0.821±0.042	0.547
	23/2			0.602
	25/2			0.436
	27/2			0.017
	29/2			1.878

structure of bands 1 and 2 around the band crossing region.

4.1.2 Negative parity bands 5 and 6

The comparison of calculated and available experimental [4] transition strength ratios $B(M1)/B(E2)$ for negative parity bands is also presented in Table 2(a). From this table, it is observed that the present calculations have nicely reproduced the transition strength ratios for negative parity yrast band for I=13/2 to I=17/2. The calculated $B(M1)/B(E2)$ values show a slow decrease with spin from I=13/2 to I=33/2 thereby, showing no abrupt change in the structure of yrast negative parity bands.

4.2 Results and discussion on transition strength ratios of ^{135,137}Sm

In case of ^{135}Sm, the experimental data on electromagnetic transition probabilities are not available. The values for $B(M1)/B(E2)$ ratios have been predicted for yrast positive parity band and are presented in Table 2(b). The calculated $B(M1)/B(E2)$ ratios show a decrease in their values from spin I=11/2 to 13/2 and after that these values are nearly constant up to spin I=21/2. At spin I=29/2, these values show an increase due to the change in structure of the yrast positive parity band after the band crossing region.

The comparison of calculated and experimental $B(M1)/B(E2)$ ratios for ^{137}Sm is presented in Table 2(c). The negative parity band which is a ground state yrast band, in this nucleus has two sets of experimental data [6,8] on $B(M1)/B(E2)$ ratios up to spin I=21/2. The observed trend of $B(M1)/B(E2)$ ratios of Ref. [8] is reasonably reproduced by the present calculation except at the spin I=19/2$^-$ as can be seen in the Table 2(c). The increase in the $B(M1)/B(E2)$ values at the spin I=19/2$^-$ is not reproduced by the present calculation. The predicted values of $B(M1)/B(E2)$ show a sharp decrease at spin I=27/2 and then an increase at spin I=29/2, which can be attributed to the alignment of protons in the down sloping K-components of $\pi(h_{11/2})^2$ orbitals.

5 Summary and conclusions

From the foregoing discussion of the calculated results and their comparison with the experimental data, the following broad conclusions can be drawn:

In ^{133}Sm all the seven experimentally known bands have been studied. The PSM calculations successfully give a deeper understanding of the mechanism of the formation of yrast and excited state bands from the single and multi-quasiparticle configurations. The positive parity ground state band based on configuration $1\nu 5/2^+[413]$ $(2d_{5/2})$, band spectra (both signature partners – bands 1 and 2) and crossing frequencies for ^{133}Sm are successfully reproduced. The present calculations have found $(h_{11/2})^2$ proton crossing at frequency (~0.400 MeV) which is an indication of structural change caused by crossing of ground state band by 3-qp bands. Experimentally, it is also observed that there is tentative evidence for the $(h_{11/2})^2$ proton crossing at a frequency (~0.35 MeV). Also, it has been found that the first excited positive parity band is based on configuration $1\nu 1/2^+[400]$ $(2d_{3/2})$, which is very much consistent with the experimental observation. The band head energy and band spectra of excited positive parity bands is not confirmed experimentally. The present calculations predict the band head energy of band 3 as 0.226 MeV with respect to band 1. The transition energies of bands 3 and 4 at lower spins are fairly reproduced by the present calculations.

Further, it has been found that 1-qp neutron band built on K=7/2 and having configuration $[523]7/2^-$ $(h_{11/2})$ is lowest in energy out of all other negative parity bands, which is very much consistent with the experimentally observed band head spin and configuration assigned to this band. The band spectra and band head spin of bands represented by 5 and 6 (signature partners of $1\nu 1h_{11/2}$) are not confirmed experimentally. However, the present calculations predict the band head energy of band 5 as 0.179 MeV with respect to positive parity band 1. The present calculations are successful in reproducing $E2$ transitions of bands 5 and 6 and dipole transitions $M1$ connecting these two bands. The decoupled band 7 in ^{133}Sm has been assigned $[541]1/2^-$ $(h_{9/2})$ configuration experimentally. The present calculation predicts band 7 as arising from $1\nu 1/2^-[541]$ $(2f_{7/2})$ configuration. The relative band head energy of this band with respect to yrast negative parity band 5 is predicted as 0.444 MeV. The present calculations reproduced the available $E2$ transitions for this decoupled band. The decrease in calculated $E2$ transitions at higher spin may be due to crossing by 3-qp bands around spin $37/2^-$.

For the reliability of wave functions, we have calculated the electromagnetic transition strength ratios for positive and negative parity yrast bands of ^{133}Sm. From the results, it is found that the calculated $B(M1)/B(E2)$ reflect a decrease in their values around the band crossing spin $31/2^+$ indicating a change in the structure of bands around this spin. Comparison of calculated transition strength ratios $B(M1)/B(E2)$ with the available experimental data is good except at the angular momentum state $13/2^+$. For negative parity yrast band of ^{133}Sm the calculated $B(M1)/B(E2)$ values do not show any significant change up to band crossing spin 33/2. The present calculations have nicely reproduced the transition ratios $B(M1)/B(E2)$s for negative parity yrast band except at spin I=11/2 in case of ^{133}Sm isotope.

In case of ^{135}Sm, 1-qp neutron band built on K=7/2 and having configuration $1\nu 7/2^+[404](1g_{7/2})$ is lowest in energy out of all other positive parity bands up to the spin

I=23/2$^+$ and is consistent with experimentally known band head spin and configuration. The crossing by 3-qp bands at the spin 25/2$^+$ causes a significant change in the yrast structure of ^{135}Sm. This crossing predicts the occurrence of backbending in the calculated results at the band crossing spin I=25/2$^+$, which is also observed experimentally at the same spin and rotational frequency. The $B(M1)/B(E2)$ ratios have been predicted for the positive parity yrast ground state band of ^{135}Sm. The present calculations in ^{135}Sm found the dominant structure of the lowest negative parity band based on K=9/2 state of the neutron $1h_{11/2}$ orbital up to the spin 13/2$^-$ and is consistent with the experimental band head spin and configuration. The calculated results of ΔI=1 transition energies and moment of inertia, for negative parity band 2 reproduces the observed staggering in this band due to the admixture of $1v1/2^-[541]$ band with low K=1/2 component in the wavefunction. As the band spectra of ^{135}Sm is tentative and not confirmed experimentally, it is not feasible to make precise comments on the agreement of the calculated results with the available experimental data.

The present calculations for negative parity of ^{137}Sm predicted that the dominant structure of yrast band up to the spin 15/2$^-$ is K=9/2 state of neutron $h_{11/2}$ orbital, which is consistent with the experimental band head spin and configuration. For the positive parity of ^{137}Sm, 1-qp neutron band from K=7/2 state of neutron orbital $g_{7/2}$ is lowest in energy from all the other positive parity bands. Experimentally, this band is proposed to originate from the K=1/2 state of neutron $d_{3/2}$ orbital. However, reasonably good agreement with the experimental energies for whole of this band supports the predicted configuration $1v7/2[404](1g_{7/2})$ for this band. The present calculations reproduced the band spectra of both positive and negative parity bands. The observed backbending phenomena have been reproduced nicely at the band crossing spins due to the crossing of 1-qp neutron bands by 3-qp bands. The backbending in moment of inertia is predicted to arise due to the alignment of pair of protons in the down slopping K-components of $\pi(h_{11/2})^2$ orbitals. For ^{137}Sm, the observed trends in $B(M1)/B(E2)$ have been reasonably reproduced except at the spin I=19/2$^-$. The calculated results on $B(M1)/B(E2)$ show the sharp increase in their values at spin I=29/2$^-$ due to the alignment of a pair of protons in the $\pi(h_{11/2})^2$ orbitals.

The present calculations well reproduced the low-spin experimental data on $^{133\text{-}137}$Sm. However, the precise position of spins and rotational frequencies where quasiparticle alignments take place are very sensitive to several calculation conditions. One of them is to select the best Nilsson-single particle states for neutron-deficient nuclei in the mass region A~130-140. The Nilsson single particle states in the present work are obtained by using the standard Nilsson parameters of Ref. [23] without any adjustment. The agreement with the experimental data may be improved further by directly modifying the Nilsson parameters for the neutron-deficient A~130-140 mass range as discussed in Ref. [31] for proton-rich nuclei in the upper pf shell.

We are thankful to Professor Y. Sun for his collaborations.

References

1 A. Galindo-Uribarri, Rev. Mex. Fis., **45-S2**: 55 (1999)
2 R. Wadsworth et al, Z. Phys. A- Atomic Nuclei, **333**: 409 (1989)
3 P. H. Regan et al, Nucl. Phys. A, **533**: 476 (1991)
4 C. M. Parry et al, Phys. Rev. C, **60**: 054314 (1999)
5 S. M. Mullins et al, J. Phys. G: Nucl. Phys., **13**: L201 (1987)
6 R. Ma et al, Phys. Rev. C, **40**: 156 (1989)
7 E. S. Paul et al, Phys. Rev. Lett, **61**: 42 (1988)
8 C. R. Alvarez et al, Nucl. Phys. A, **624**: 225 (1997)
9 Y. -C. Yang and Y. Sun, Mechanics and Astronomy, Science China, **54**: 81 (2011)
10 Y. -C. Yang, Y. Sun, S. J. Zhu et al, Nucl. Part. Phys, **37**: 085110 (2010)
11 K. Hara and Y. Sun, Int. J. Mod. Phys. E, **4**: 637 (1995)
12 Y. Sun and K. Hara, Comp. Phys. Commun, **104**: 245 (1997)
13 Y. Sun, Phys. Scr, **91**: 043005 (2016)
14 K. Hara and Y. Sun, Nucl. Phys. A, **531**: 221 (1991)
15 K. Hara and S. Iwasaki, Nucl. Phys. A, **332**: 61 (1979)
16 K. Hara and S. Iwasaki, Nucl. Phys. A, **348**: 200 (1980)
17 K. Hara and Y. Sun, Nucl. Phys. A, **529**: 445 (1991)
18 K. Hara and Y. Sun, Nucl. Phys. A, **537**: 77 (1992)
19 P. Ring and P. Schuck, *The Nuclear Many Body Problem*, (Springer- Verlag, Berlin, 1980)
20 I. L. Lamm, Nucl. Phys. A, **125**: 504 (1969)
21 V. Velazquez, J. Hirsch, and Y. Sun, Nucl. Phys. A, **643**: 39 (1998)
22 Y. Sun, S. X. Wen, and D. H. Feng, Phys. Rev. Lett., **72**: 3483 (1994)
23 T. Bengtsson and I. Ragnarsson, Nucl. Phys. A, **436**: 14 (1985)
24 P. Moller, A. J. Sierk, T. Ichikawa et al, At. Data and Nucl. Data Tables, **109-110**: 1 (2016)
25 P. Moller, J. R. Nix, W. D. Myers et al, At. Data and Nucl. Data Tables, **59**: 185 (1995)
26 B. Singh, A. A. Rodionov, and Y. L. Khazov, Nucl. Data Sheets, **109**: 517 (2008)
27 E. Browne and J. K. Tuli, Nucl. Data Sheets, **108**: 2173 (2007)
28 Y. L. Khazov A. A. Rodionov, and F. G. Kondev, Nucl. Data Sheets, **112**: 855 (2011)
29 A. Ibanez-Sandoval et al, Phys. Rev. C, **83**: 034308 (2011)
30 Y. Sun and J. L. Egido, Nucl. Phys. A, **580**: 1 (1994)
31 Y. Sun, J.-y. Zhang, M. Guidry et al, Phys. Rev. C, **62**: 021601(R) (2000)